UNIVERSITY OF CALIFORNIA
RIVERSIDE

The Role of Bacterial Biofilms in Chronic Infections

A Dissertation submitted in partial satisfaction
of the requirements for the degree of

Doctor of Philosophy

in

Biomedical Sciences

by

Danh Cong Do

December 2014

Dissertation Committee:
Professor Neal L. Schiller, Chairperson
Professor Manuela Martins-Green
Professor Dimitrios Morikis

The Dissertation of Danh Cong Do is approved:

_____

_____

_____
Committee Chairperson

University of California, Riverside

ACKNOWLEDGEMENTS

"No one has a monopoly on wisdom or knowledge. We can always learn from each other". Pope Francis.

First, I would like to acknowledge my PhD thesis committee members, Dr. Neal L. Schiller, Dr. Manuela Martins-Green, and Dr. Dimitrios Morikis. Your guidance, time, and support have been monumental to my success here at UC Riverside. I learned so much from all of you throughout these years and for that, you have my greatest appreciation and thanks.

More specifically, I would like to acknowledge my major professor, Dr. Neal L. Schiller. Thank you for your guidance and support in all of these years and thank you for allowing me the freedom to seek, explore, and be creative in the scientific topics that most excite me. To me, you are a mentor, a teacher, and most importantly, a friend.

In addition, I would like to acknowledge my colleagues, Brandon Gallaher, Sandeep Dhall, and Zied Gaieb, without whom this work cannot be possible. Your collaboration and friendship means so much to me. Thank you and good luck in your future endeavors.

Lastly, I would like to acknowledge the many professors, staff, and students in the Program of Biomedical Sciences in the School of Medicine. Your involvement has made my time here at UC Riverside far more enjoyable than I could have imagined. Thank you.

DEDICATION

I dedicate this thesis to my Father and Mother, Phillip Thuan Cong Do and Hoa Thi Nguyen. Your love, support, and hard work have been a source of inspiration and motivation for me throughout my entire life. I also dedicate this thesis to my siblings: Kevin Thanh and his family, Derek Dat, Loan Anh, Phuong Anh, John Nam-Hoai, and Nhung. Your constant involvement in my life is a blessing. Remember to follow your dreams, trust in yourself, and find guidance from the people that went before you as you embark on your education and life journey. Lastly, I dedicate this thesis to Anh-Thu, the love of my life. Your patience, support, and love throughout my graduate education have been invaluable. Together we can do anything. I look forward to our life together in the near future.

ABSTRACT OF THE DISSERTATION

The Role of Bacterial Biofilms in Chronic Infection

by

Danh Cong Do

Doctor of Philosophy, Graduate Program in Biomedical Sciences
University of California, Riverside, December 2014
Dr. Neal L. Schiller, Chairperson

Biofilm is the virulence factor that is responsible for chronic infection in diseases such as Cystic Fibrosis (CF) and chronic wounds. In this thesis, we examine the role of AlgX, a required protein for alginate biosynthesis in *P. aeruginosa*. We show that the absence of AlgX resulted in the loss of mucoidy and *in silico* studies demonstrated that AlgX binds alginate. Alanine mutations demonstrated that K396, T398, W400, and R406 are important for alginate binding. Alginate rescue assays confirm the importance of these amino acid residues for alginate biosynthesis and acetylation. This is the first functional demonstration of AlgX role in alginate biofilm biosynthesis and acetylation.

Biofilm-producing bacteria and redox imbalance are the leading factors that turn acute wounds into chronic wounds. We demonstrated that LIGHT$^{-/-}$ mouse wounds contain elevated levels of reactive oxygen species (ROS). To see whether chronic wounds can be generated, we increased the redox imbalance in the LIGHT$^{-/-}$ wounds and infecting the wounds with biofilm-forming bacteria. We demonstrated that by using these conditions, we could induce chronic wounds in the LIGHT$^{-/-}$ mouse model 100% of the

time. These wounds do not re-epithelialize, contain high bacterial burden, and sustained multi-species bacterial infections that are biofilm-forming and antibiotic-resistant.

We also demonstrated that increasing the redox imbalance was sufficient to turn *db/db* wounds into chronic wounds. These wounds sustained spontaneous biofilm-producing bacterial infections. To verify that redox imbalance is critical for chronicity, we treated chronic wounds with antioxidants and found that oxidative stress was highly reduced, biofilm production was decreased, and bacteria became more sensitive to antibiotics. This is the first demonstration that chronic wounds can be generated and reversed by manipulating the wound's redox microenvironment in an animal model.

Norspermidine has been shown to negatively affect the structure of extracellular polymeric substances (EPS). Using the bacteria that colonized *db/db* chronic wounds, we demonstrated that 2 mM norspermidine reduces the amount of adherent biofilms produced by exudate bacterial communities. Furthermore, application of norspermidine increases the bactericidal effect of gentamicin. We believe that norspermidine could be used in combination with bactericidal antibiotics to control biofilm infection in dermal chronic wounds.

TABLE OF CONTENTS

LIST OF FIGURES

LIST OF TABLES

CHAPTER 1

Bacterial biofilms and its implications in chronic infections

Scientific Review and Background

Bacterial life can be found on nearly all surfaces of this planet and predominately exists as a microbial mass that flourishes in a slimy layer adhered to a surface. This microbial mass is termed "biofilm"; biofilms can form anywhere where there is a surface with some moisture and nutrients (1). The existence of biofilm has been known for quite some time now due to the fact that many biofilms are sufficiently thick enough to be seen by the naked eye (2). However, it was not until 1970 that we began to understand that bacteria in biofilms exist predominately as sessile bacteria and it is not until another decade that we began to appreciate that adhered bacteria in biofilms are organized in elaborate ways (3). For example, one bacterial species that is attached to a surface can co-aggregate with many partners of the same species or of different species, which themselves can aggregate with other partners to form a dense bacterial mass. This type of bacterial co-aggregation and organization is called a microcolony (2) and bacterial biofilms consisting of microcolonies on a surface constitute a protected mode of growth that allows survival in a hostile environment. Such complexity of biofilm structure has led to the analogy of biofilms to tissues of higher organisms (4).

Of clinical importance, bacteria in biofilms can withstand host immune responses, and they are much less susceptible to antibiotics compared to their non-biofilm counterparts (5). Furthermore, even in individuals with normal cellular and humoral immune reactions, biofilm-associated infections are rarely resolved by the hosts' defense systems (2). In addition, aggressive antibiotic therapy often only reverses the symptoms associated with planktonic bacteria that are released from the biofilm, but often fails to

kill the biofilm itself (6). This makes biofilm-associated infections difficult to treat and almost impossible to eradicate.

Many of the infectious diseases that affect immune-compromised individuals involve bacterial species that are commonly found on the human body or are ubiquitously found in the environment. For example, patients with Cystic Fibrosis (CF) have a mucosal immunodeficiency that resulted in bacterial colonization in the lungs predominated by *Pseudomonas aeruginosa*, a bacterium that is commonly found in the soil, water, and air (7). Chronic infection in the lungs of CF patients often resulted the phenotypic conversion of *P. aeruginosa* into a mucoid phenotype. This mucoid phenotype results from the production of a specific biofilm called alginate. Alginate producing *P. aeruginosa* eludes phagocytosis and is resistant to antibiotics and many therapeutic agents. In addition, alginate is immunogenic and elicits immune responses that result in the production of antibodies and many reactive oxygen species without resulting in the clearance of the organisms (8-10). The failure of the immune systems to clear the infection and the predominance of alginate-producing *P. aeruginosa* is the pathogenic factor that result in the morbidity and mortality of patients with CF.

The biofilm alginate is one of the most studied biofilms in *P. aeruginosa*. The biosynthesis of alginate can generally be divided into four different phases: [1] the synthesis of precursor substrate, [2] the polymerization and secretion across the cytoplasmic membrane, [3] periplasmic transfer and modification, and [4] excretion across the outer membrane into the extracellular space (11). The initial step of alginate biosynthesis is centered on the modification of the sugar metabolite, mannose 6-

phosphate, into the alginate precursor GDP-mannuronic acid (12). This step is catalyzed by both the bifunctional enzyme phospho-mannose isomerase (PMI)/guanosine-diphospho- mannose pyrophosphorylase (GMP), designated AlgA, and the phosphomannomutase AlgC (13, 14). The second step is predicated around the polymerization of GDP-mannuronic acid monomers into polymannuronate, which is catalyzed by a cytoplasmic membrane embedded protein, called Alg8. Alg8 is thought to both polymerize monomers of GDP-mannuronate and secrete its polymannuronate products into the periplasm (15). The third step involves an array of proteins (AlgG, AlgL, AlgK, AlgX, AlgI, AlgJ, and AlgF) that are important for alginate modification and binding (16, 17). Many of these proteins have well defined functions except for AlgX, a protein with a relatively unknown function, which appears to be required for alginate production (18, 19). It was proposed that AlgX, AlgK, Alg44, AlgG, and AlgL formed a protein scaffolding complex within the periplasm that modified, protected, and guided nascent alginate chains to AlgE, the final step of alginate biosynthesis (16). Previously, our lab has shown that AlgX is a required component for alginate biosynthesis. Chromosomal deletion of *algX* in the mucoid inducible CF clinically isolated *P. aeruginosa* FRD1 strain resulted in the loss of mucoidy (or biofilm) due to the production of low-molecular weight (LMW, <30KDa) uronic acid (UA) in place of high-molecular weight UA polymers, also refered to as alginate. (19-21). Thus, we proposed that the production of LMW UA is due to the unregulated degradation of HMW UA by AlgL, the alginate lyase. In a recent study, *P. aeruginosa* AlgX crystal structure revealed that AlgX is a two-domain protein consisting of a SGNH hydrolase-like domain and a

carbohydrate-binding module. Experimental data suggested that the SGNH hydrolase-like domain might play a direct role in alginate acetylation (22). However, the role of its carbohydrate-binding module in terms of biofilm alginate biosynthesis still remains elusive.

As mentioned previously, biofilm associated bacterial infections in the lungs of CF patients are extremely difficult to manage. The deleterious effects of bacterial infection and the adverse effects of bacterial biofilms on wound healing are well known (23). It been recognized that controlling bioburden and disrupting the biofilm are important aspects of wound management that could lead to better wound healing outcomes (24). Great efforts have been dedicated to addressing these aspects; however, research over the past two decades has shown that many chronic biofilm-associated infections are rarely resolved by the immune defenses and respond transiently to antimicrobial therapy (2, 4, 25). For example, the skin bacterium *Staphylococcus epidermidis* can infect the wounds of compromised hosts and *S. epidermidis* cultured from tissue taken from difficult-to-heal, delayed healing, and chronic dermal wounds show the presence of biofilm bacteria surrounded by an exopolysaccharide matrix (2, 26). Furthermore, the infections of these wounds are often associated with biofilm that may be composed of a single species or by a mixture of species of bacteria. These biofilm producing bacterial communities are insensitive to host immune responses, antibiotics, and many therapeutic agents.

The role of biofilm has been known to prevent wounds from healing, however, direct evidence of biofilm involvement in chronic wound infections is scarce. Numerous

animal models of chronic wounds have been developed, however, these models poorly resemble human chronic wound pathophysiology (27-30). Recently, we documented that, occasionally, wounds from the tumor necrosis factor super-family member 14 deleted mouse ($LIGHT^{-/-}$), a mouse with a delayed wound healing phenotype, become chronic. These chronic wounds surprisingly sustained spontaneous chronic biofilm-producing *S. epidermidis* infection (31, 32). In further analysis of the microenvironment of the wounds, we believe that elevated concentrations of reactive oxygen species (ROS) coupled with the presence of biofilm producing bacteria are responsible for pushing the wounds toward chronicity. To demonstrate this, we increased the ROS levels in the wounds by inhibiting specific key redox detoxifying enzymes and applied the previously isolated biofilm-producing *S. epidermidis* directly to the wounds of $LIGHT^{-/-}$ mouse. In doing so, we were able to create $LIGHT^{-/-}$ chronic wounds 100% of the time. Hence, we have provided additional evidence for the involvement of bacterial biofilms in the formation of chronic wounds. Given our observations, it will be crucial to determine whether the same conditions that were used to trigger the formation of chronic wounds in the $LIGHT^{-/-}$ animal can be applied to other animal models of delayed wound healing (i.e. *db/db* mouse of type II diabetes).

Given the recent advances in wound care and management, chronic wounds still remain a huge problem in the United States and costs approximately $25 billion dollars annually (33). Bacterial biofilms haave been suggested to be the underlying factor that prevent wounds from healing and microbial control has been recognized as an important aspect of chronic wound management. Although the series of events leading to the

development of chronic wounds remains unclear, redox imbalance/stress caused by elevated concentrations of reactive oxygen species (ROS) followed by the presence of biofilm-producing bacteria have been suggested and in studies demonstrated by us to play key roles in the process (23, 31, 34-36). Therefore, it is conceivable that targeting ROS stress and bacterial biofilms could consequently lead to a better wound-healing outcome.

It has been shown that ROS are generated soon after injury by resident endothelial cells and fibroblasts soon after injury (37). Low levels of ROS are essential mediators for proper wound healing and are required for the defense against invading pathogens (38, 39). However, high levels of ROS are known to cause DNA damage, gene dysregulation, and cell death creating a propitious environment for bacterial infection (39). Studies have demonstrated that high levels of ROS in non-healing ulcers in humans are often infected with many bacterial species (i.e. *Staphylococcus aureus, Enterococcus faecalis, P. aeruginosa,* coagulase-negative staphylococci and *Proteus* species) (34, 40-42). Therefore, a fine ROS balance is required for proper wound healing, which is not observed in wounds that become chronic. Given that many antioxidants agents, such as N-acetyl cysteine and α-tocopherol, have been shown to be protective against oxidative stress (43); it is conceivable to believe that these antioxidants agents can be used to abate redox stress in chronic wounds and potentially result in a better wound healing phenotype. However, the use of these antioxidant agents in promoting chronic wounds healing has yet to be evaluated.

It has been emphasized over and over again that biofilm-producing bacteria play key roles in preventing wounds to heal (23, 31, 34-36). Much is known about the

assembly of biofilm (i.e., *P. aeruginosa* alginate biofilm), however, its dispersion still remains largely elusive. It been proposed that three key features are required for the dispersal of biofilms. One, there must be a change in the gene expression profile of bacteria in the biofilm toward a dispersal-promoting manner. Such dispersal-promoting cues could come from stress signal sensing within the biofilm or by the surrounding environment. Two, the signaling cues must diffuse to the nearby surrounding bacterial biofilm masses, establishing an effective communication network that enables effective coordinative disassembly. Such molecular cues are probably mediated via small signaling molecules. Finally, the encapsulating bacteria must detach and disperse from the extracellular matrix to allow the release of cells into the environment (44-46). This mode of disassembly must be made possible by the existence of endogenous soluble factors that mediate biofilm dispersion. One such molecule is the polyamine norspermidine, which has been shown to reduce the amounts of adherent biofilm from *E. coli* and *S. aureus in vitro* (45). This is the first evidence suggesting that small molecule inhibitors may be used to combat biofilm-associated infections in chronic wounds.

In summary, bacterial biofilms are implicated in both the infection of the wounds (i.e., like those in the lungs of CF patients or the ulcers on diabetic individuals) and in the failure of those wounds to heal. Identifying events leading to the development of chronic wounds and understanding the conditions in which biofilms are formed and dispersed will potentially lead to the development of diagnostic molecules and new therapeutics for the treatment of chronic wounds. Such information is of immense importance in the management of chronic wounds as well as to produce the most positive clinical outcome

and/or the prevention of infection. The studies presented in this thesis will advance our understanding of the unique biology of bacterial biofilms in chronic infections and hopefully lay the groundwork for further studies in the advancement of chronic wound care.

CHAPTER 2

AlgX carbohydrate binding module is required for the biosynthesis of alginate in Pseudomonas aeruginosa

Abstract

Alginate encapsulated *Pseudomonas aeruginosa* is the primary causative agent of respiratory insufficiency and failure in patients with cystic fibrosis. AlgX is a protein that is required for alginate biosynthesis and has been suggested to participate in alginate acetylation. We demonstrate that in the absence of AlgX, 92% of alginate polymers produced by the *algX*-deleted mutant are subsequently degraded by AlgL, a periplasmic alginate lyase that is responsible for cleaving misguided alginate polymers. Using alginate affinity assays and molecular docking studies, we demonstrate that AlgX binds alginate via the carbohydrate-binding module located in the C-terminal region. Alanine mutations of the predicted amino acid residues that interact with alginate suggest that K396, T398, W400, and R406 are important for alginate binding. Alginate rescue assays using *in trans* expression of mutated AlgX (with single amino acid substitution) in the *algX*-null background and quantification of uronic acid O-acetylation in these mutants confirms the importance of the AlgX CBM domain for alginate synthesis. These observations suggest that the AlgX CBM acts as an intermediate shuttle to guide nascent alginate polymers toward the acetylation machinery and eventually to AlgE.

Introduction

Cystic fibrosis (CF) is a chronic, progressive, and often fatal genetic inherited disease caused by mutations in the gene that encodes the CF transmembrane conductance regulator (CFTR) protein (47-49). CF is the predominant genetic disorder in Caucasians. The hallmark of CF is the excessive loss of salt during sweating and the production of abnormally thick mucus in the lungs due to inadequate mucociliary clearance, which facilitates respiratory infections (50). Persistent infection by alginate-producing or mucoid *Pseudomonas aeruginosa* is the leading cause of death in CF patients (50-52). Alginate is an exopolysaccharide consisting of acetylated or non-acetylated mannuronic and guluronic acid polymers (53). Alginate-producing *P. aeruginosa* are resistant to many antibiotics, protected from oxidative stress, and insensitive to host immune clearance (54-56). These characteristics make alginate producing *P. aeruginosa* infection in CF lungs difficult to treat and almost impossible to eradicate.

Conversion of *P. aeruginosa* into a hyper alginate-producing strain (i.e., mucoid phenotype) is predominately associated with inactivation of the *mucA* gene by spontaneous mutations (57). The *mucA* gene codes for the anti-sigma factor MucA and with MucB, forms a two-component regulation complex (MucA-MucB) that post-transcriptionally controls the activity of the alternative sigma factor AlgU (also called AlgT and σ^{22}). In CF lungs, there is a strong tendency for mutations in *mucA* that results in the bypass of the circuitry that controls the activity of AlgU/σ^{22} (58-61) leading to the constituent activation of the *algD* operon producing the mucoid phenotype. The *algD* operon contains proteins that are required for the production of the alginate precursor

GDP-mannuronic acid and the catalysis of alginate polymerization, modification, and export, as well as various auxiliary proteins required for the production of mature alginate (58, 62-66).

The *algD* operon is composed of *algD*, *alg8*, *alg44*, *algK*, *algE*, *algG*, *algX*, *algL*, *algI*, *algJ*, *algK*, and *algA*. The *algD* and *algA* genes encode for the expression of a GDP-mannose dehydrogenase (AlgD) and phosphomannose isomerase/GDP-mannose pyrophosphorylase (AlgA), and with the phosphomannomutase (AlgC) are responsible for the production of GDP-mannuronic acid monomers (14, 67-70). The inner membrane embedded Alg8 protein (encoded by *alg8*) catalyzes alginate polymerization and AlgE is an alginate specific porin protein (encoded by *algE*) that enables the export of nascent alginate chains through the outer membrane (11, 53, 71-74). Alg44 is a transmembrane protein (encoded by *alg44*) that binds bis-(3'-5')-cyclic dimeric guanosine monophosphate and is thought to be important for the proper linkage/positioning of Alg8 and AlgE (11, 15). The alginate modification machinery, composed of AlgG (mannuronan C-5-epimerase), AlgL (alginate lyase), and AlgI, AlgJ, and AlgF (O-acetylation) is encoded by the *algG*, *algL*, *algI*, *algJ*, and *algF* genes, respectively (75-81). AlgK contains three putative domains that promote protein-protein interactions and is thought to be the scaffolding protein for the assembly of the alginate biosynthetic components within the periplasm (82, 83).

The *algX* gene encodes a 53KDa protein that localizes to the periplasm and is required for alginate biosynthesis (18, 19). It was proposed that AlgX, AlgK, Alg44, AlgG, and AlgL formed a protein scaffolding complex within the periplasm that

modified, protected, and guided nascent alginate chains to AlgE (16). Chromosomal deletion of *algX, algG, or algK* in the mucoid inducible CF clinically isolated *P. aeruginosa* FRD1 strain (FRD1050) resulted in the production of low-molecular weight (LMW, <30KDa) uronic acid (UA) polymers (19-21). Immunoprecipitation assays using Strep-tag II fusion AlgX demonstrated that AlgX interacts with AlgK (84). The crystal structure of AlgX revealed a protein that contains a N-terminal SGNH hydrolase-like domain and a C-terminal carbohydrate-binding module (22, 85). Mutation of the Ser-His-Asp triad in the N-terminal SGNH hydrolase-like domain resulted in the production of non-acetylated alginate (22). This is the first structural characterization of AlgX and its involvement in alginate acetylation.

In this chapter, we quantified the different populations of uronic acid polymers produced by the *P. aeruginosa algX*-deleted mutant (FRD 2-2) and its parental strain (FRD1050). Using an alginate column affinity assay, we confirmed that AlgX could bind alginate. Using *in silico* docking studies, we identified the region of AlgX responsible for alginate binding. Using alanine mutations and *in trans* complementation in an *algX*-deletion mutant, we examined the importance of specific amino acid residues in AlgX for alginate binding, biosynthesis, and acetylation.

Materials and Methods

Bacterial strains, plasmids, and reagents. The list and characteristics of all bacterial strains and plasmids used in this study are shown in Table 2.1 (see page 16). *Escherichia coli* strains were routinely cultured in Luria broth (LB) (BD Difco, Sparks MD) or Luria agar (LA) (BD Difco) plates at 37^{o}C in a humidified incubator with antibiotic as required. *P. aeruginosa* strains were cultured in modified alginate producing (MAP) media (20) or *Pseudomonas* Isolation Agar (PIA) (BD Difco) with 5.0% v/v glycerol (Fisher BioReagents, Fair Lawn NJ) at 37^{o}C in a humidified incubator with antibiotic as required. Selection was carried out using the following antibiotic concentrations: tetracycline (Sigma-Aldrich, St. Louis MO) at 25μg/mL (Tc_{25}) for *E. coli* and 100μg/mL (Tc_{100}) for *P. aeruginosa*; gentamicin (Sigma-Aldrich) at 50μg/mL (Gm_{50}) for *P. aeruginosa* or 25μg/mL (Gm_{25}) if used together with Tc_{100}, and kanamycin (Sigma-Aldrich) at 100μg/mL (Kn_{100}) for *E. coli*. The CF clinically isolated *P. aeruginosa* FRD1 with the *algD* promoter replaced with an inducible P*tac* promoter (FRD1050) was kindly provided by Dr. Dennis Ohman (80). The creation of an inducible *P. aeruginosa* FRD1050 *algX*-deleted mutant (FRD 2-2) was described previously (19). The non-mucoid ubiquitous environmental *P. aeruginosa* PAO1 strain (86) was used as a control when necessary. The hexa-histidine (His_6) tag was blotted using a rabbit anti-His-tag polyclonal antibody (Cell Signaling, Danvers MA) at 1:2000 v/v dilution. Detection of AlgX and AlgL was carried out using rabbit serum antibody previously created by our group (19, 76) at 1:2000 v/v dilution.

Table 2.1: Bacterial strains and plasmids used in this study		
Strains or plasmid	Phenotype and/or genotype	Reference or source
***P. aeruginosa* strains**		
FRD1050	Prototrophic, alginate positive CF isolate; *algD* operon controlled by *tac* promoter; Cb^r	43
FRD 2-2	*algX* deletion mutant derivative of FRD1050; the gentamicin cassette replaces part of *algX;* Cb^r	18
FRD 2-2::*XHis*$_6$	FRD 2-2 transformed with pUC21T*algXHis*$_6$ or pUCP21T*algXHis*$_6$ containing single site directed amino acid mutation	This study
***E. coli* strains**		
DH10β	F^- *mcr*AΔ(*mrr-hsdRMS-mcrBC*) Φ80*lac*ZΔM15 Δ*lac*X74 *deo*R *rec*A1 *ara*D139 Δ(*ara-leu*)7697 *gal*U *gal*K *rps*L(Str^r) *end*A1 *nup*G *fhu*A::IS2	Invitrogen
HMS174(DE3)pLysS	F^- *rec*A *hsd*R (rk12- mk12-) Rif^r (DE3) pLysS Cm^r	56
HB101	*sup*E44 *hsd*S20(r^-_B m^-_B) *rec*A13 *ara*-14 *pro*A2 *lac*Y1 *gal*K2 *rps*L20 *xyl*-5 *mtl*-1	56
GeneHogs®	F^- *mcr*AΔ(*mrr-hsdRMS-mcrBC*) Φ80*lac*ZΔM15 Δ*lac*X74 *rec*A1 *ara*D139 Δ(*ara-leu*)7697 *gal*U *gal*K *rps*L(Str^r) *end*A1 *nup*G	Invitrogen
Plasmids		
pUCP21T	Broad-host-range expression vector, Ap^r, contains 1.9-kb *PstI* fragment from pRO1614, ori, lac promoter containing the tetO/tetR cassette cloned upstream of the ori using *AlfII*	55
pUCP21T*algXHis*$_6$	pUCP21T containing *P. aeruginosa* FRD1 *algXHis*$_6$ ORF, some with single site directed mutation, into the MCS using 5'*Xba*I and 3'*Bam*HI	This study

Abbreviations: Cb^r, carbenicillin resistance; Cm^r, chloramphenicol resistance; Ap^r, ampicillin resistance; Tc^r, tetracycline resistance; *mob*+, mobilizable plasmid.

DNA manipulation. FRD1050 genomic DNA was extracted and purified using the DNeasy Blood and Tissue kit (QIAGEN, Gaithersburg MD). Purified DNA was used as the template to amplify the *algX* open-reading frame (ORF) via PCR amplification. PCR amplification was carried out with either Platinum Pfx DNA polymerase mix (Invitrogen, Grand Island NY) or 2.0X Apex Taq RED Master Mix (Genesee Scientific, San Diego CA) with 3.0% v/v DMSO (Sigma- Aldrich). The following primers were used to amplify the *algX* carboxyl-terminal hexa-histidine fusion tag (*algXHis$_6$*) ORF: Xba+1*algX* (5'AAA AAA AGC TCT AGA GAT GAA AAC CCG CAC TTC CCG) and 3'*algX*His$_6$ (5'CGC CGC GGA TCC TTA GTG GTG ATG GTG ATG ATG CTT AAG CCT CCC GGC CAC CGA CTG GCT). Primers were purchased from Integrated DNA Technologies (IDT, San Diego CA). DNA fragments were separated using agarose gel electrophoresis and purified using Wizard SV Gel kit (Promega, Madison WI). PCR amplified products were purified using the PCR Clean-up System (Promega). The *algXHis$_6$* ORF was cloned into pUCP21T in frame with the upstream *pLac* promoter using *Bam*HI (New England Biolabs, Ipswich MA) and *Xba*I (New England Biolabs) restriction sites creating pUCP21T*algXHis$_6$*. pUCP21T*algXHis$_6$* was transformed into *E. coli* HMS174(DE3)pLysS (87) and *E. coli* GeneHogs® (Invitrogen, Grand Island NY) using electroporation (88). Triparental mating (89) was used to transform *P. aeruginosa* strains using *E. coli* HB101 (87) as the helper strain.

Site-directed mutagenesis was achieved using the Q5 site-directed mutagenesis kit (New England Biolabs). Briefly, *algXHis$_6$* point mutations were introduced into pUCP21T*algXHis$_6$* by PCR, as instructed by the manufacturer, using primers generated

by NEBaseChange™: R364A+Q5SDM (5'GCG CCA GGG CGC CAA CGA GGT GC), R364A-Q5SDM (5'AGC TTG ACC TTG CGG CTG), K396A+Q5SDM (5'ACA CGA GTT GGC GAA CAC CAT CTG GTA C), K396A-Q5SDM (5'ACC GAA GGG TCG CTG TAG), T398A+Q5SDM (5'GTT GAA GAA CGC CAT CTG GTA CAT G), T398A-Q5SDM (5'TCG TGT ACC GAA GGG TCG), W400A+Q5SDM (5'GAA CAC CAT CGC GTA CAT GAA CGG CC), W400A-Q5SDM (5'TTC AAC TCG TGT ACC GAA G), R406A+Q5SDM (5'GAA CGG CCG CGC CGA GCA GTT G), R406A-Q5SDM (5'ATG TAC CAG ATG GTG TTC), K410A+Q5SDM (5'CGA GCA GTT GGC GAT CGA GCA GTC GAA AG), and K410A-Q5SDM (5'CGG CGG CCG TTC ATG TAC). The mutated pUCP21T*algXHis*$_6$ point mutant DNA was treated with the KLD enzymes mixture provided by the manufacturer and transformed into NEB 5α chemicompetent *E. coli* cells using temperature shock. Cells were selected on LB/Tc$_{50}$ agar plates overnight at 37^{o}C in a humidified incubator. Mutagenesis was confirmed by sequencing the pUCP21T*algXHis*$_6$ point mutant using the following primer *algX* 630+ ('5GCG CGT CGG CCT GCT GTC CA) at the University of California at Riverside Institute for Integrative Genome Biology.

Alginate rescue assay. FRD 2-2 was transformed with pUCP21T*algXHis*$_6$, or pUCP21T*algXHis*$_6$ bearing either the R364A, K396A, T398A, W400A, R406A, or K410A mutation via electroporation or triparental mating. Potential transformants were plated onto PIA/Gm$_{25}$/Tc$_{100}$ plates and grown at 37°C in a humidified incubator until colonies appeared. Transformants were screened for the plasmid of interest via PCR using the following DNA primers: Primer pUC19 3150- (5'GGT GCG GGC CTC TTC

GCT) is specific to the downstream end of the multiple cloning sites in pUCP21T in the reverse orientation and *algX* 430+ (5'TAC GAC TCG CGC TAC AAC AC) is specific to *algX* in the forward direction. Screening for FRD 2-2 genomic background was carried out as described by Robles-Price et al (19). Transformed FRD 2-2 colonies were subcultured either on PIA/Gm_{25}/Tc_{100}/$IPTG_{0.5mM}$ plates or in MAP/Gm_{25}/Tc_{100}/$IPTG_{0.5mM}$ media for 12-24hr. Cells grown on agar plates were scraped and resuspended in 1mL Tris-NaCl buffer (25mM Tris pH 7.6 and 140mM NaCl). Cells were separated from the liquid cultures by centrifugation at 16,783xg for 10min at 4°C and supernatants were collected. To quantify the production of high molecular (HMW, >30 KDa) and low molecular weight (LMW, ≤30 KDa) UA polymers, the culture supernatants were passed through a 30 KDa Amicon® Ultra-15 Centrifugal filter (Millipore, Billerica MA). The flow-through fractions and un-filtered supernatant were collected and uronic acid content was determined using the Carbazole assay (90).

AlgXHis$_6$ expression, isolation, and purification. *E. coli* HMS174(DE3)pLysS containing pUCP21T*algXHis$_6$* was grown in 2mL of LB/Tc_{25} overnight at 37°C/200RPM and then used to inoculate a 250mL LB/Tc_{25} culture the following day. The culture was grown to an optical density at 595nm (OD_{595nm}) of 0.7-0.8 and $AlgXHis_6$ expression was induced using 0.5mM of isopropyl-β-D-thiogalactopyranoside (Sigma-Aldrich) at 37°C/200RPM for 12-16hr. Bacterial cells were harvested by centrifugation at 8,240xg for 15 min at 4°C then washed three times with cold Tris-NaCl buffer (25mM Tris pH 7.6 and 140mM NaCl). Cells were suspended in cold lysing buffer (Tris-NaCl buffer containing 1mM dithiothreitol, 1mM phenylmethanesulfonyl fluoride, 200μg/mL of

lysozyme, and 3% v/v glycerol) at 100mg of cell-wet weight to 1mL of lysing buffer and incubated at 4°C for 2-3hr with rocking. DNA was sheared by sonication using a Vibra Cell CV250 (Sonics and Materials, Newtown CT) for 3 cycles (15sec continuous pulse at 50% duty cycle on ice per cycle). Insoluble materials were removed by centrifugation (20 min at 4°C at 12,900xg) and soluble supernatant was filtered through at 0.45μm-pore-size filter (Millipore, Billerica MA).

AlgXHis_6 purification was carried out using Ni-NTA His-Bind resin (Novagen, San Diego CA). To equilibrate the resin, 50% Ni-NTA His-bind slurry was mixed with binding buffer (25mM Tris pH 7.6, 140mM NaCl, 200mM KCl, 1mM imidazole, and 1mM β-mercaptoethanol) at a v/v ratio of 1:4. The slurry was then allowed to settle by gravity and the supernatant was then removed. The same volume was added back to the equilibrated slurry using cleared lysate-containing AlgXHis_6. The solution was mixed gently and incubated at 4°C for 2hr with shaking. The slurry-lysate solution was then loaded onto a chromatography column and allowed to empty by gravity at room temperature at a rate of 1 drop per second. The slurry packed column was then washed twice with 4mL of washing buffer (25mM Tris pH 7.6, 140mM NaCl, 200mM KCl, 1mM β-mercaptoethanol, and 20mM imidazole) and emptied via gravity flow. The flow-through fractions were saved. To elute the bound proteins, four 1mL fractions of elution buffer (25mM Tris pH 7.6, 140mM NaCl, 200mM KCl, 1mM β-mercaptoethanol, and 200mM imidazole) were added to the column and the gravity flow-through fractions were saved and analyzed by SDS-PAGE and Western blot.

Quantification of unsaturated uronic acid polymers. *P. aeruginosa* strains FRD1050 and FRD 2-2 were grown in 2mL of MAP media overnight at 37^{o}C/200RPM with the appropriate antibiotics. The resulting cells were used to inoculate a 50mL culture using MAP media with the appropriate antibiotics and then grown to an OD_{595nm} of 0.7-0.8 before induction with 0.5mM of IPTG for 8hr. Cells were collected by centrifugation at 12,900xg for 30min at 4^{o}C and supernatants were removed. LMW UA polymers from IPTG induced FRD1050 and FRD 2-2 culture supernatants were isolated as previously described. To determine the concentrations of reduced uronic acids, a byproduct of AlgL catalysis, we measured the TBA activity of known concentrations of *P. aeruginosa* FRD1050 ethanol precipitated alginate (91) that was incubated with AlgL (isolated from FRD1050 periplasm) at RT overnight. From these data points, we generated a standard curve equating the TBA colorimetric intensity (OD_{548nm}) and the concentration of AlgL digested alginate (Figure 2.1C). Isolated LMW UA polymers were assayed for reduced sugar ends using the TBA reagents.

Cross-linking P. aeruginosa FRD1050 alginate to EAH Sepharose 4G resin. An alginate resin was created by cross-linking *P. aeruginosa* FRD1050 ethanol precipitated alginate (91) onto EAH Sepharose 4B beads (GE Healthcare, Pittsburgh PA) using 1-ethyl-3-[3-dimethylaminopropyl]carbodiimide hydrochloride (EDC). In brief, 4mL of EAH Sepharose 4B beads were washed three times with 10mL of acidified deionized water (pH 4.5) and then resuspended in 10mL of acidified deionized water containing 500mM NaCl. Purified FRD1050 alginate was resuspended in 25mM HEPES buffer pH 4.5 to a concentration of 30μg/mL and then mixed at 1:1 v/v ratio with the washed

Sepharose 4B beads. Alginate-to-beads conjugation was catalyzed at 4°C with drop-wise addition of 2mL of a 1.0M solution of EDC dissolved in 25mM HEPES pH 4.5. The reaction was then incubated for 2hr in a rotating platform at 4°C. The pH was monitored and adjusted to 4.0-5.0 using diluted solution of HCl or NaOH as needed. The resins were collected by centrifugation at 3,200xg for 30min at 4°C and washed three times with 10mL of Tris buffer pH 7.6. The Carbazole or TBA assay was used to determine whether conjugation was successful (53).

Alginate affinity assay. No alginate-conjugated (null slurry) and alginate-conjugated Sepharose 4B resins were used to pack 0.7x5.5cm chromatography columns (BioRad) to a bed height of 1.50-1.75cm. A 0.75mL solution of purified $AlgXHis_6$ (input) was passed by gravity through the alginate conjugated or null slurry resin and the flow-through fractions were collected. The columns were washed three times with 0.75mL of 25mM Tris buffer pH 7.6 and wash flow-through fractions were collected. Sepharose beads were then resuspended with 0.75mL of 25mM Tris buffer pH 7.6 containing 0.1% v/v β-mercaptoethanol. Proteins were eluted off the beads by boiling the samples for 30min and the supernatant was collected after centrifugation at 2000xg for 15min. Collected fractions were standardized by volume and blotted for $AlgXHis_6$ using SDS-PAGE and Western blot. Nitrocellulose blots were developed using BCIP/NBT Substrate Solution (PerkinElmer, Boston MA) and imaged using an 8 megapixels iSight camera under normal laboratory illumination on white background. The digital RBG images were converted to 8-bit (256 gray shades) and densitometric analysis of $AlgXHis_6$ was quantified using ImageJ 1.47v (Mac OSX version, http://imagej.nih.gov/ij).

Measurement of density profile was done by volume (average band intensity multiplied by its area) and the presence of $AlgXHis_6$ was calculated as percentage relative to input.

O-acetylation assay. Alginates were isolated by ethanol precipitating (91) uronic acid polymers produced by the IPTG induced FRD 2-2 complemented with pUCP21T harboring either a non-mutated or alanine mutated *algXHis*$_6$. Uronic acid (UA) concentrations from isolated alginates were determined using the Carbazole assay (90). Quantification of O-acetylation from the isolated alginates was carried out using a scaled-down version (22) of a chemical method first described by Hestrin (92).

Structure modeling. The three-dimensional coordinates of the crystallographic structure of AlgX were obtained from the Protein Data Bank (PDB) using the PDB code 4KNC (22). AlgX was crystallized as a dimer with both molecules missing some residues due to the quality of electron density in the region. Glu-447 and Asp-250:Ser-251 were missing from the selected protein. We obtained the full protein sequence from www.uniprot.com and aligned it to the sequence with missing residues obtained from the PDB, excluding the N-terminal and C-terminal loops that are not relevant for our study, using ClustalW2 (93). The alignment was used to generate a structure of AlgX with the missing residues using Modeller (94). Modeller has been shown to be very effective for short loops (95). The two missing segments, consisting of one and two amino acids, are located in solvent-exposed flexible loops, for which dynamic interconversion of multiple local conformations is expected; the conformations of the modeled three amino acids are representative within a locally optimized microenvironment.

Crystal structures of UA polysaccharides, MMM, ΔMMM, and ΔMMGM, were extracted from PDB structures 2PYH, 1HV6, and 1Y3P, respectively (96-98). These structures were used as starting structures to generate different polysaccharide combinations of mannuronic (M) and guluronic (G) acid in the presence or absence of reducing ends (Δ). Polysaccharide combinations were generated using Chimera. Autodock Vina v1.1 (99) was used to dock our constructed alginate polymers into the carbohydrate-binding module of AlgX. We prepared the ligands to dock using AutoDockTools (100) by adding polar hydrogens to both the ligand and receptor, setting all single bonds of the ligand as rotatable, and saving both files as pdbqt files. The search space was reduced to the C-terminal carbohydrate-binding module of AlgX within a grid box of 27.5 x 41.75 x 34.3 Å.

After preparing the ligands and receptor and defining the binding site grid box, we used Autodock Vina to generate 20 models for each ligand at an exhaustiveness of 100 with a series of optimization tests provided by the Autodock Vina protocol. Models docked within the pinch point (22) of the CBM were selected for further analysis. Resulting receptor-ligand complexes were analyzed using computational scripts to determine the percent occupancies of AlgX residues involved in Alginate binding. The scripts were written in R (101) using the Bio3D v2.0 package and UCSF Chimera v1.8.1 (102). The occupancies represent the percentage of complexes that harbor a specific interaction between a residue in AlgX and a saccharide subunit in the docked ligand, from the complexes generated with Autodock Vina v1.1 and have ligands bound at the pinch point. The complexes were examined to determine the presence of hydrogen bonds

and salt bridges. Hydrogen bonds were extracted using the Chimera software and salt bridges were calculated using a cutoff value of 5 Å between the charged functional groups (102).

Statistical analysis. All data are expressed as the mean average of at least three independent replicates ± standard deviation (StDev). A two-tailed Student's *t*-test was used to compare values obtained from two independent groups. p-Values ≤ 0.05 were considered statistically significant. Statistical comparisons were reported as p-Value $\leq$ 0.05 (*), p-Value $\leq$ 0.01 (**), and p-Value $\leq$ 0.001(***); NS = not significant.

Results

AlgL cleaves nascent alginate produced by the algX-deleted mutant. We have previously reported that AlgX is required for alginate biosynthesis *in P. aeruginosa* and chromosomal deletion of *algX* (FRD 2-2) in the FRD1050 parental strain resulted in a loss of mucoidy due to the production of LMW UA polymers in place of alginate or HMW UA polymers (18, 19). Furthermore, we reported that LMW UAs isolated from FRD 2-2 were highly reduced (19) suggesting that the production of LMW UA polymers is likely due to AlgL cleavage of alginate in the periplasm. In this study, we quantified the relative abundance of LMW and reduced LMW UA polymers (rLMW), a product of AlgL degradation by β-elimination (103) from FRD 2-2. Although both FRD1050 and FRD 2-2 produce almost the same amount of UA, FRD 2-2 produces exclusively LMW UA polymers (720±53μg/mL) compared to FRD1050, which produced a mixture of LMW (255+12μg/mL) and HMW (515±25μg/mL) UA polymers (Figure 2.1A/B). Using alginate purified from the periplasm of FRD1050 that has been completely degraded by AlgL (expressing 37±3 EU/mg-min lyase activity), we demonstrated that there is a linear relationship between the colorimetric intensity in the TBA assay and the concentration of AlgL digested alginate (Figure 2.1C). We determined that, of the total LMW UA mass isolated from FRD 2-2, 92% of the LMW UA polymers are reduced. In addition, we determined that 83% of the LMW UA polymers isolated from FRD1050 are reduced (Figure 2.1D). These observations confirm that in the absence of AlgX (FRD 2-2), no intact HMW UA polymers are transported out of the cell because AlgL degrades alginate polymers in the periplasm. In the presence of AlgX and an intact alginate biosynthetic

scaffold (FRD1050), about ⅔ of the alginate (HMW UA) polymers are transported into the supernatant or to AlgE intact; however, AlgL can still digest the occasionally misguided or periplasm-exposed polymer (about ⅓ of alginate is LMW).

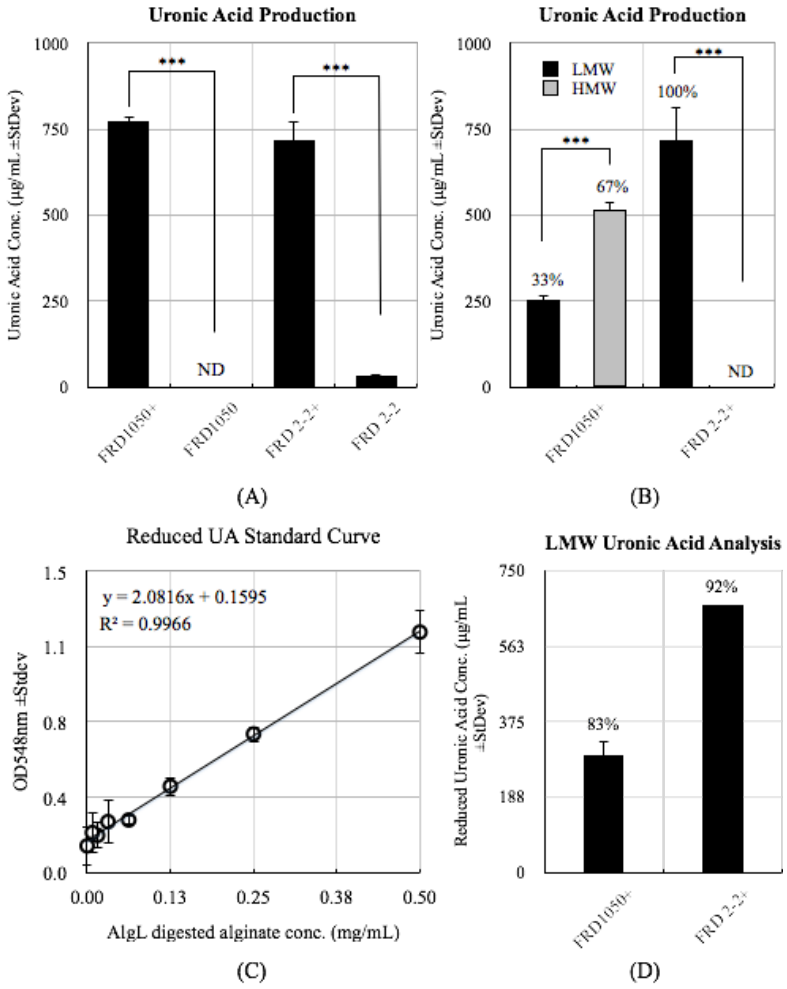

Figure 2.1: Quantitation of uronic acid production. (A) Total uronic acid (UA) production was quantified for FRD1050 and FRD 2-2 in the presence (+) or absence of IPTG. IPTG induced FRD1050 and FRD 2-2 produce similar amounts of UA. (B) UA polymers from FRD1050 and FRD 2-2 after IPTG induction (+) were separated into LMW (<30KDa) and HMW (>30KDa) polymers and then quantified using the Carbazole assay (53). FRD1050 produces a mixture of LMW and HMW UA and FRD 2-2 produces exclusively LMW UA. Relative amounts of LMW and HMW UA are also reported as percentage of total UA obtained. (C) The mass of reduced uronic acid was calculated by using the relationship between the TBA colorimetric intensity and the relative concentrations of AlgL digested alginate. (D) LMW UA from FRD1050 and FRD 2-2 were assayed for reduced ends as described in the Materials and Methods. % shown represents % of total LMW UA produced with reduced ends. This observation suggests that the LMW UA produced by FRD1050 and FRD 2-2 contain exclusively reduced ends, a product of alginate lyase cleavage of alginate polymers. ND indicates no detectable signal.

In silico data indicate that alginate docks to the carbohydrate-binding module. The crystal structure revealed that AlgX is a two-domain protein containing a N-terminal SGNH hydrolase-like domain and a C-terminal carbohydrate-binding module (CBM). The superposition of AlgX CBM domain with CBM29-2 (PDB code 1GWK) in complex with a mannohexose ligand indicated a set of four highly conserved amino acid residues (R364, T398, W400, and R380) dubbed the substrate recognition pinch point (SRPP) (22). Given the differences in the architectural makeup of the alginate polymer, mainly by the presence of guluronic acid residues, we sought to refine the conformational binding motif of AlgX and to provide additional insight into secondary contributions from other amino acid residues. Using *in silico* modeling, we docked a variety of alginate polymers consisting of various permutations of mannuronic and guluronic acid monomers (Figure 2.2A) to the CBM. The alginate polymers docked into the SRPP domain of the CBM produced a wide range of conformational poses. Calculating the interaction occupancies provided the statistical significance of the interactions between specific AlgX amino acid residues and the alginate polymers (Figure 2.2B). K396, R406, and K410 have hydrogen-bonding occupancies of 88%, 88%, and 100%, respectively, in our generated conformational poses. R364 has a calculated hydrogen-bonding occupancy of 19%. Salt bridge occupancies of R364 and R406 interacting with the docked polymers show relatively modest occupancy percentages (30% and 60% respectively) while K396 and K410 have high percentage of salt bridge occupancies (100% and 90% respectively). T398 and W400 were predicted to form low or no hydrogen bonding with a calculated percent occupancy of 13% and 0% respectively. This shows that among four of the

proposed amino acid residues that make up the putative SRPP, only R406 is shown to form high intermolecular interaction with the docked alginate polymers while T398 and W400 may be contributing more in aliphatic interactions. K396 is calculated to form hydrogen bonding and salt bridges in 88% and 100% of our poses. Similarly, K410 has relatively high hydrogen bonding and salt bridges occupancy (100% and 90%). Given our docking observations, we hypothesized that K396 and K410 may also directly interact with the alginate polymer. The topology of R364, K396, T398, W400, R406, K410, and an example of a docked ligand (MGMMGM) is shown in Figure 2.2C. The Figure shows that R364, K396, and R406 surround the ligand contributing to hydrogen bond- and salt bridge-mediated binding. Contact occupancies were also observed for many additional amino acid residues; however, these contact points are situated outside the CBM and were not considered to be potentially important for alginate binding.

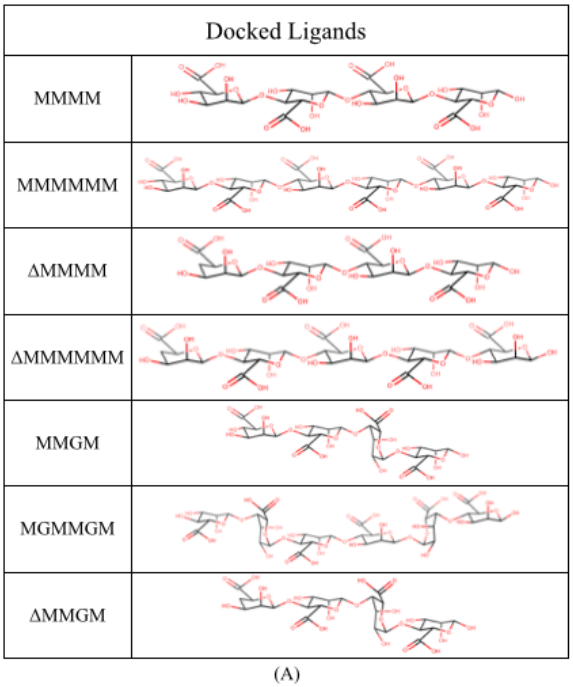

Calculated Percent Occupancy		
AA	H-bond	Salt Bridges
R364	19%	30%
K396	88%	100%
T398	13%	NA
W400	0%	NA
R406	88%	60%
K410	100%	90%

(B)

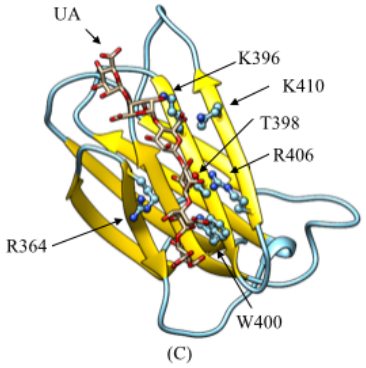

Figure 2.2: In silico docking of alginate ligands to AlgX carbohydrate binding module (CBM). (A) Variations of uronic acid polysaccharides composed of mannuronic (M) and guluronic (G) acid generated for the docking studies; some contain reduced ends (Δ). The chemical structures of the polysaccharides were drawn using MarvinSketch 6.2.1 (ChemAxon; http://www.chemaxon.com/). (B) Intermolecular interaction occupancies of docked alginate ligands to AlgX CBM domain. Percent occupancies of selected amino acid residues that harbor a specific hydrogen bond or salt bridge interaction between a residue in AlgX and a saccharide subunit in the molecule docked. Hydrogen bonds were calculated using the Chimera criteria (65). Salt bridge occupancies are a subset of the listed hydrogen bonds, and were calculated using a 5-Å cutoff value between charged functional groups. NA = not applicable. (C) Molecular model of the CBM (in ribbon representation) with the amino acids examined for contributions to polysaccharide binding in complex with a representative uronic acid (UA) polysaccharide (MGMMGM).

AlgX binds alginate and alanine substitution of K396, T398, W400, and R406 affects AlgX binding. To date only AlgG and AlgL have been demonstrated to bind alginate (20, 76). To determine whether AlgX could bind alginate, we passed purified $AlgXHis_6$ through an alginate cross-linked Sepharose 4B column and analyzed the flow-through fractions using SDS-PAGE and western blot (Figure 2.3). Densitometric analysis of captured flow through fractions revealed that the alginate cross-linked Sepharose 4B column retained 67±26% of the input $AlgXHis_6$ compared to 37±6% from the null column (beads without alginate). After three washings, both columns lost approximately equal percentage of input $AlgXHis_6$ (17±8% and 20±7%). Eluting $AlgXHis_6$ from the columns, we calculated that 50±11% of input $AlgXHis_6$ was retained by the alginate cross-linked Sepharose 4B column compared to 16±4% from the null column (Figure 2.3A). These observations indicated that $AlgXHis_6$ binds alginate.

Our docking study indicates that in addition to the amino acid residues that make up the SRPP, K396 and K410 may also participate in binding alginate. To determine whether alanine substitutions of R364, K396, T398, W400, R406, and K410 would affect alginate binding, individually purified $AlgXHis_6$ mutants bearing the respective alanine substitution were passed through the alginate cross-linked Sepharose 4B column and flow-through fractions were analyzed for $AlgXHis_6$ via SDS-PAGE and Western blotting. Densitometric analysis demonstrated that alanine substitution of K396, T398, W400, and K406 significantly affect $AlgXHis_6$ retention in the alginate cross-linked Sepharose 4B column (Figure 2.3A) compared to the non-mutated $AlgXHis_6$. The percentage of $AlgXHis_6$ retained by the alginate column in respect to the input was

33±7% and 12±3% for the K396A and R406A mutant, respectively, compared to 50±11% for the non-mutated $AlgXHis_6$. Alanine mutation of T398A completely eliminated $AlgXHis_6$ ability to bind alginate. Alanine mutation of W400 significantly increases the retention of $AlgXHis_6$ (96±8%) by the alginate cross-linked Sepharose 4B column. The retention percentages of R364A and K410A are 39±9% and 50±11%, respectively, suggesting that R364 and K410 do not significantly affect $AlgXHis_6$ binding to alginate.

Alanine substitution of T398, W400, and R406 affects alginate biosynthesis. To determine whether changes in alginate binding would affect alginate biosynthesis, we tested the ability of these $AlgXHis_6$ mutants to reconstitute alginate production by comparing the relative percentages of HMW UA polymers produced by the complemented FRD 2-2. *In trans* expression of $AlgXHis_6$ in FRD 2-2 bearing either the T398A, W400A, or R406A mutations produce HMW UA polymers with levels that are significantly lowered (42±9%, 31±2%, and 40±22% respectively) than that compared to non-mutated $AlgXHis_6$ (72±2%). The K396A mutation resulted in a marginal but significant decrease in alginate binding and reconstituted HMW UA production in FRD 2-2 at levels similar (76±1%) to that observed in the non-mutated $AlgXHis_6$ (73±1%). This could be due to the salt bridge or hydrogen bonding compensatory effect of K410, which sits proximally to K396 in the adjacent alpha helix (Figure 2.2C). The R364A and K410A mutants did not significantly affect $AlgXHis_6$ binding to alginate and produce HMW UA polymer at levels (80±19% and 73±1%) that are comparable to that of the non-mutated $AlgXHis_6$ (Figure 2.3B).

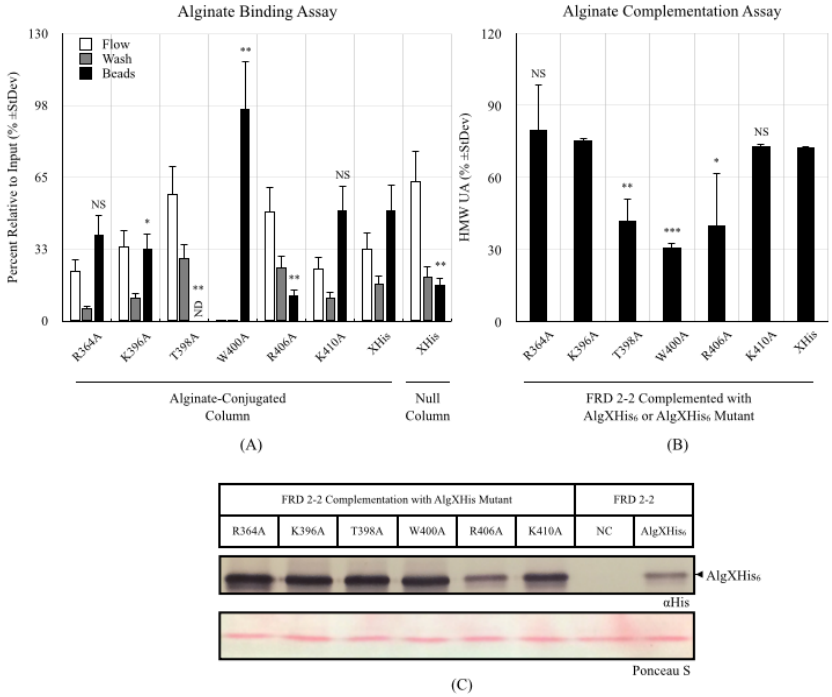

Figure 2.3: Alginate affinity assay and HMW uronic acid quantitation of FRD 2-2 by complementation with AlgX or its alanine mutants. (A) The retention of $AlgXHis_6$ (XHis) by the alginate cross-linked Sepharose 4B column and its presence in captured flow through fractions were analyzed using ImageJ 1.47v with the built-in densitometric analysis plugin. The percentage of $AlgXHis_6$ retained by the null column (Null) serves as a non-specific binding baseline value. The retention percentages of alanine mutated $AlgXHis_6$ bearing the R364A, K396A, T398A, W400A, R406A, and K410A were compared to the retention percentage obtained from the $AlgXHis_6$ non-mutated sample. Flow: input fraction that was captured after a single pass through the column. Wash: the sum of $AlgXHis_6$ found in the three wash fractions. Beads: the percentage of $AlgXHis_6$ retained by the column. ND indicates not detected. (B) The ability of $AlgXHis_6$ bearing either the R364A, K396A, T398A, W400A, R406A, or K410A mutations to rescue alginate production in FRD 2-2 was quantified by comparing the percentage of HMW UA polymers produced by the mutants to the non-mutated $AlgXHis_6$. (C) The expression of the various $AlgXHis_6$ mutants was demonstrated by blotting for the hexa-histidine tag via Western blotting from complemented FRD 2-2 cellular extracts. Total proteins were stained using Ponceau S on nitrocellulose membrane after transfer. NC = not complemented.

Alanine substitution of T398, W400, R406, and K410 affects alginate acetylation. To determine whether alginate acetylation is affected due to the changes in the ability of the $AlgXHis_6$ mutants to bind alginate, we quantified the degrees of O-acetylation from UA isolated from FRD 2-2 complemented with the $AlgXHis_6$ mutants. $AlgXHis_6$ mutants bearing the T398A, W400A, and R406A substitution resulted in a significant decrease in alginate acetylation compared to non-mutated $AlgXHis_6$ (Figure 2.4). FRD 2-2 complemented with the T398A, W400A, or R406A resulted in respectively 0.13±0.04, 0.10±0.03, and 0.08±0.03mM of acetylated UA-per-mM total UA (mM^A/mM^T) compared to 0.24±0.05mM^A/mM^T for the non-mutated $AlgXHis_6$. Interestingly, alginate acetylation was not affected by the mutation of K396 into alanine (0.24±0.09mM^A/mM^T), although, we previously observed a significant reduction in alginate binding. In contrast, the mutation K410A, which does not contribute to alginate binding, significantly affected alginate acetylation (0.11±0.05mM^A/mM^T). This demonstrated that K396 participation in alginate binding is not important for acetylation and K410 does not participate in alginate binding but is important for acetylation. We did not observe a significant change in alginate acetylation for the R364A mutant (0.17±0.05mM^A/mM^T).

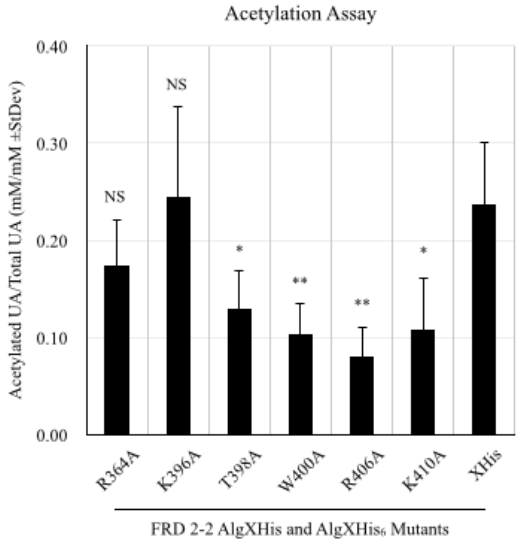

Figure 2.4: Quantitation of O-acetylated UA from FRD 2-2 complemented with AlgXHis$_6$ mutants. Purified UA from FRD 2-2 complemented with AlgXHis$_6$ mutants were assayed for O-acetylation. Values obtained from the point mutants were compared to FRD 2-2 complemented with the non-mutated AlgXHis$_6$.

Discussion

Previously we reported that AlgX is required for alginate biosynthesis and its absence resulted in the loss of mucoidy due to the production of LMW UA polymers (18, 19). Structural and functional characterization suggests that mutation of the catalytic triad in the N-terminal SGNH hydrolase-like domain resulted in non-acetylated alginate (22). This is the first structural characterization of AlgX participation in polysaccharide acetyltransferase. However, the role of the C-terminal carbohydrate-binding module (CBM) of AlgX has not been evaluated. In this study we show that 100% of the LMW UA polymers produced by FRD 2-2 and its parental FRD1050 strain are a result of enzymatic degradation by AlgL. Alginate affinity assays demonstrated that AlgX has the ability to bind alginate. Docking studies and alanine mutations suggest that K396, T398, W400, and R406 are essential for alginate binding. Furthermore, we also demonstrated that mutation of the amino acid residues that participate in alginate binding directly affects alginate biosynthesis and alginate acetylation.

UA polymers produced by the *algX*-deleted mutant, dubbed FRD 2-2, contain high amounts of reduced sugar ends. We concluded that this population of LMW UA is due to the degradation of alginate polymers by AlgL (19). To provide additional evidence for this conclusion, we quantified the mass of LMW UA and demonstrated that 92% of the LMW UA polymers produced by FRD 2-2 are reduced suggesting that they are products of AlgL degradation. Furthermore, AlgL contains a signaling peptide that localizes to the periplasm (76, 104) suggesting that degradation occurs in the periplasm. Interestingly, the production of a small population of reduced LMW UA polymers in

FRD1050 implies that AlgL functions as an alginate scavenging protein that occasionally degrades misguided polymers during alginate biosynthesis.

Previously published work demonstrated the presence of a network of residues in the CBM of AlgX that could accommodate a single hexamannose polysaccharide (22). This network, dubbed the substrate recognition pinch point (SRPP), was composed of two basic residues (R364 and R406), an aromatic (W400), and a polar (T398) residue. Architecturally, the alginate polymer differs from the hexamannose polysaccharide due to the presence of guluronic acid residues that cause the alginate polymer to bend. To accommodate for this structural difference, we used various combinations of UA ligands composed of mannuronic and guluronic polymers as substrates for our docking studies. From our *in silico* modeling, we demonstrated that many of the amino acid residues that were reported by Riley et al. (22) have high calculated percentage of hydrogen bond formation and salt bridge occupancy. Among the proposed amino acid residues that made up the SRPP (R364, T398, W400, and R406), alanine mutation of T398 and R406 resulted in a significant reduction in alginate binding (See Table 2.2). In addition, mutation of K396 significantly reduced AlgX binding to alginate. In contrast, the alanine substitution of W400 significantly increased alginate binding. Our observations suggest that T398 may be important for substrate recognition and acts to situate the alginate polymer inside the SRPP, and that amino acid residues K396, R406, and W400 stabilize the polysaccharide-protein complex by the formation of hydrogen bonds, salt bridges and aliphatic interactions. Our data largely agrees with the previously published predictions (22).

It is uncertain whether the CBM domain of AlgX plays a role in alginate biosynthesis. Site-specific mutations in the CBM that resulted in the greatest change in alginate binding (i.e., T398, W400, and R406) significantly reduce alginate production and alginate acetylation (Table 2.2). Therefore, it is conceivable that the CBM serves as an intermediary alginate-shuttling domain whose function is to guide and direct the nascent alginate polymers, acting as an extension to the acetylation complexes given that AlgI, AlgJ, and AlgF lack a carbohydrate-binding domain (77, 79). Such ligand-binding modules have been known to enhance substrate affinity as well as stabilization and are often appended to catalytic machinery (105, 106).

In this chapter, we have demonstrated that AlgX binds alginate and site-directed mutations of the amino acids located in the CBM SRPP that participate in polysaccharide binding affect AlgX affinity to alginate. In addition, we also demonstrated that the alginate-binding quality of AlgX CBM is important for alginate biosynthesis and acetylation. During alginate biosynthesis, we believe that AlgX CBM acts as an intermediate shuttle that guides the nascent alginate polymer toward the acetylation machinery and eventually to AlgE. This is the first functional demonstration of AlgX's CBM role in alginate biosynthesis and acetylation.

	Alginate Binding	HMW UA Production	Alginate Acetylation
XHis	+	+	+
R364A	+	+	+
K396A	R	+	+
T398A	-	R	R
W400A	++	R	R
R406A	R	R	R
K410A	+	+	R

Table 2.2: Characteristic observations of AlgXHis$_6$ mutants: Binding to alginate, alginate rescues (HMW UA production), and alginate acetylation outcomes obtained from AlgXHis$_6$ mutants were compared to non-mutated AlgXHis$_6$ (XHis). No statistical differences or similar outcomes compared to XHis are indicated by (+). A statistically significant increase compared to XHis is indicated by (++). A statistically significant decrease is indicated by (R). A complete loss of activity is indicated by (-).

CHAPTER 3

Bacterial biofilms, redox stress, and the creation and reversal of mouse chronic wounds

Abstract

Human chronic wounds, such as diabetic foot, pressure and venous ulcers, and other similar chronic wounds, impact ~6.5M people and cost ~$25B/year in the US alone. While great efforts have been made to stimulate healing of these wounds, success has been limited. The purpose of this study is to determine the factors that trigger the wound on a path to chronicity. We report that the inhibition of two reactive oxygen species antioxidant systems soon after injury and the topical infection with biofilm-producing bacteria resulted in the formation of chronic wounds in the mouse LIGHT knock out ($LIGHT^{-/-}$) animal model. In a more clinically relevant animal model, the diabetic (*db/db*, type II) mouse model, we demonstrated that early inhibition of the same reactive oxygen species antioxidant systems alone is sufficient to create chronic wounds with spontaneously biofilm-producing bacterial infection, presumably arising from the animal skin's microbiome. These chronic wounds ($LIGHT^{-/-}$ and diabetic) are infected with biofilm-producing bacteria largely made up of coagulase-negative *Staphylococcus sp.*, *Enterococcus sp*., *Enterobacter cloacae*, and *Pseudomonas sp*. We also demonstrated that by abating redox stress (treating the chronic wounds with the antioxidants, α-tocopherol and N-acetyl cysteine) in the diabetic wounds, we were able to achieve better healing with reduction in biofilm-forming bacterial burden. In conclusion, we show for the first time that by inhibiting specific reactive oxygen species antioxidant systems with or without biofilm-producing bacterial infection, we are able to create chronic wounds in two different animal models. Furthermore, we demonstrated that wound chronicity can be reversed by abating redox stress in the diabetic animal model. Our findings demonstrate

the importance of reactive oxygen species balance and skin microbiota that will help in deciphering the mechanisms underlying the development of chronic wounds and hence find potential targets to treat them.

Introduction

Wound healing is a dynamic process that comprises a sequence of phases and is regulated by a variety of environmental conditions and by different growth factors, cytokines, and hormones. Defects in the healing process, or failure of acute wounds to proceed through the normal regulated repair process, result in wounds that have impaired healing and/or become chronic (107, 108). Great efforts have been made to alter the course of repair from non-healing wounds to healing wounds; however, success has been limited. This is chiefly due to the lack of animal models that resemble human chronic wounds.

We recently showed that a mouse in which the Tumor Necrosis Factor Superfamily Member 14 (TNFSF14/LIGHT) gene has been knocked out ($LIGHT^{-/-}$ mice) has wounds that heal poorly and show many of the characteristics of impaired wounds in humans (31). When compared to wounds in normal animals (controls), the wounds of $LIGHT^{-/-}$ mice show defects in epithelial-dermal interactions, high degree of inflammation, and damaged microvessels with virtually no basement membrane or periendothelial cells. The collagen in the granulation tissue is mostly degraded; matrix metalloproteinases (MMPs) are elevated and tissue inhibitors of metalloproteinase (TIMPs) are down-regulated. In addition, we also found that the $LIGHT^{-/-}$ wounds occasionally become chronic, and when they do, these defects are highly accentuated. In addition, the wounds become heavily infected with *Staphylococcus epidermidis* (31), a gram-positive bacterium frequently found in human chronic wounds (109).

Diabetic foot ulcers and other similar chronic wounds impact ~6.5M people and cost ~$25B/year in the US alone (33). Patients with diabetes often have defects in the healing process and are at high risk of developing non-healing ulcers. The critical need for a cure of chronic wounds is underlined by the continuous increase in type II diabetes accounting for more than 90% of all diabetes. Although the series of events leading to the development of chronic wounds remains unclear, redox imbalance/stress caused by elevated concentrations of reactive oxygen species (ROS) and the presence of biofilm-producing bacteria potentially play key roles in the process (23, 31, 34-36). ROS are generated by resident endothelial cells and fibroblasts soon after injury (37) and low levels of ROS act as essential mediators of intracellular signaling that leads to proper healing and is required for defense against invading pathogens (38, 39). However, high levels of ROS are known to cause DNA damage, gene dysregulation, and cell death while creating a propitious environment for bacterial infection (39). Studies have provided evidence that non-healing ulcers in humans have high levels of redox stress (i.e., oxidative and nitrosative stress) (34, 40, 41) and are often infected with *Staphylococcus aureus, Enterococcus faecalis, Pseudomonas aeruginosa,* coagulase-negative staphylococci and *Proteus* species (42).

In this chapter we demonstrate that by inhibiting the activity of glutathione peroxidase (GPx) and catalase, two antioxidant enzymes, and the topical application of biofilm-producing *Staphylococcus epidermidis* C2, a bacterium previously isolated from a chronic wound (31), immediately after wounding cause the impaired wounds from LIGHT$^{-/-}$ animals to become chronic 100% of the time. In addition, LIGHT$^{-/-}$ chronic

wounds often developed secondary bacterial infections with many species commonly found in human chronic wounds. Using the *db/db* mouse model, we show that by inhibiting the same antioxidant enzymes immediately after wounding, we were able to generate chronic wounds containing spontaneously formed antibiotic-resistant bacterial biofilms. These biofilms often contain a microbial mass made up of many bacterial species and these bacterial species undergo dynamic changes over time. Moreover, we demonstrated that the bacterial burden is greatly reduced and wound chronicity can be reversed by treatment with the antioxidants N-acetyl cysteine (NAC) and α-tocopherol. These models emphasize the importance of ROS antioxidant systems and the contribution of biofilm-associated bacterial infection in the development of chronic wounds. Furthermore, these models can potentially lead to identifying diagnostic molecules and to the development of new therapeutics for chronic wounds.

Materials and Methods

Dermal excisional wound model. The generation of LIGHT$^{-/-}$ chronic wounds was performed using 12–16 week old LIGHT$^{-/-}$ mice. The procedure was performed as previously described (31). The creation of chronic wounds was carried out using 6-7 month-old *db/db* mice (homozygous for the diabetes spontaneous mutation Lepr^{db}) purchased from the Jackson laboratory (Bar Harbor, ME). Prior to wounding, the midline hairs on the back of the mouse were removed using Nair Hair Remover 24hr prior to wounding. A single full-thickness wound (excision of the skin and the underlying panniculus carnosus) was made using a 7mm biopsy punch. *Db/db* chronic wounds were induced by inhibiting the catalase and peroxidase antioxidant systems. Catalase activity was irreversibly inhibited by 3-amino-1,2,4-triazole (ATZ) via intraperitonial injection at a concentration of 1g/kg body weight 20min prior to creating the excisional wound. ATZ binds irreversibly to the protein part of catalase and is covelently attached to the protein (110). Glutathione peroxidase activity inhibition was done using mercaptosuccinic acid (MSA) topically at a concentration of 150mg/kg body weight immediately after wounding. MSA is a strong and specific reversible inhibitor of the glutathione peroxidase enzyme (111). The wound was immediately covered with sterile tegaderm (3M, St. Paul, MN). Similar treatment was carried out using age-matched C57BL/6 mice. Animals were housed at the University of California, Riverside (UCR) vivarium. All experimental protocols were approved by the UCR Institutional Animal Care and Use Committee (IACUC).

Superoxide dismutase, hydrogen peroxide, and catalase activity assay. Extracts obtained from tissues collected at various time points (4h, 12h, 24h and 48h post-wounding) were processed for total superoxide dismutase (SOD) activity using a commercially available kit (Cayman Chemical, Catalog# 706002, Ann Arbor, USA) as instructed by the assay kit manufacturer. The kit measures all three types of SOD (Cu/Zn, Mn^{-}, and EC-SOD). One unit of SOD is defined as the amount of enzyme needed to cause 50% dismutation of the superoxide radical. A standard curve was generated by measuring SOD activity of bovine erythrocytes at various concentrations run under the same conditions. SOD activities were calculated from the linear regression of the standard curve. Tissue hydrogen peroxide (H_2O_2) levels were measured by using a commercially available kit (Cell Technology Inc., Catalog# FLOH 100-3, Mountain View, USA). The assay is based on the peroxidase-catalyzed oxidation by H_2O_2 of the nonfluorescent substrate 10-acetyl-3,7-dihydroxyphenoxazine to a fluorescent resorufin. Fluorescent intensities were measured at 530nm (excitation)/590nm (emission) using a Victor 2 microplate reader. Concentrations of H_2O_2 were determined from a standard curve generated with known concentrations of H_2O_2. Tissue catalase activity was measured by using a commercially available kit (Cayman Chemical, Catalog# 707002, Ann Arbor, USA). The enzyme assay for catalase is based on the peroxidative function of catalase with methanol to produce formaldehyde in the presence of an optimal concentration of H_2O_2. The generated formaldehyde was measured spectrophotometrically at 540nm in a 96-well plate. Tissue glutathione peroxidase (GPx) activity was measured using a commercially available kit (Cayman Chemical, Catalog# 703102, Ann Arbor, USA). The activity was measured

indirectly by a coupled reaction with glutathione reductase (GR). The rate of decreasing absorbance (measured at 340nm) at 1-min intervals for a total of 5min using a Victor 2 microplate reader is directly proportional to the GPx activity of the sample. GPx activity was expressed as nmol/min/ml of tissue extract.

Bacterial isolation and characterization. Wound exudates/secretions were collected using sterile cotton swabs and resuspended in 1.0% w/v proteose peptone and 20.0% v/v glycerol solution. Bacteria were cultured for 16-18h at 37^{o}C on tryptic soy agar plates, BD Difco (Sparks, MD), containing 5.0% v/v defibrinated sheep blood, Colorado Serum Company (Denver, CO), and 0.08% w/v Congo red dye, Aldrich Chemistry (St.Louis, MO). Colonies were differentiated and isolated based on size, hemolytic pattern, and Congo red uptake. Resulting cultures were examined using Gram stain and visualized with optical microscopy. Gram-negative rods were characterized using the API®20E identification kit, Biomerieux (Durham, NC), and oxidase test, Fluka Analytical (St. Louis, MO). When required, the *Pseudomonas* Isolation Agar culture test, 42^{o}C growth test in tryptic soy broth (TSB), BD Difco (Sparks, MD), and motility assay were used. Gram positive coccal cultures were differentiated based on catalase activity, coagulation activity, Fluka Analytical (St. Louis, MO), 6.5% w/v NaCl tolerance test, and hemolytic activity. Biofilm production was quantified using methods described previously (112).

Viable bacterial cells count: Wound exudates were resuspended in sterile LB to yield a 1:4 v/v ratio of exudate-to-TSB solution. Bacterial colonies were visually counted on typticase soy agar plates containing 5% v/v sheep red blood cells incubated at 37^{o}C overnight in a humidified incubator.

Community minimal inhibitory concentrations assay. Wound exudates (containing bacteria) seeded on flat-bottomed tissue culture plates for 3-4hr at 37^{o}C in a humidified incubator were challenged with antibiotic for 12hr at various concentrations in TSB. Optical density at 595nm (OD595nm) was used to quantify bacterial growth. The community Minimal Inhibitory Concentration (cMIC) is defined as the lowest concentration of antibiotic that resulted in ≤ 50% increase in OD595nm compared to that recorded before introduction of antibiotic.

Scanning Electron Microscopy: Tissues collected were fixed in 4% paraformaldehyde for 4hr at room temperature. Samples were then dehydrated in 25%, 50%, 75%, 95% and 100% ethanol for 20min each at room temperature. Critical point drying of the tissues was performed using Critical-point-dryer Balzers CPD0202 followed by Au/Pd sputtering for 1min in the Sputter coater Cressington 108 auto. The coated samples were attached to carbon taped aluminum stubs and were imaged using an XL30 FEG scanning electron microscope.

Statistical analysis. All data are expressed as the mean of at least three independent replicates ± standard deviation (Stdev). A two-tailed Student's *t*-test was used to compare values obtained from two independent groups. A p-Value ≤ 0.05 was considered statistically significant. Statistical comparisons were reported as p-Value ≤ 0.05 (*), p-Value ≤ 0.01 (**), and p-Value ≤ 0.001(***); NS = not significant.

Results

High levels of ROS stress and the presence of bacteria resulted in the development of chronic wounds in the LIGHT$^{-/-}$ animal model. A schematic illustration of the oxidation and nitrosative stress cycle is shown in Figure 3.1. The inhibition of two mitochondrial hydrogen peroxide detoxification systems, glutathione peroxidase (GPx) and catalase (113, 114), were carried out by the irreversible AZT and highly specific but reversible MSA molecules, respectively. To determine whether the use of these inhibitors of antioxidant enzymes (IAE) in LIGHT$^{-/-}$ wounds will result in further increase in oxidative stress, we measured the levels of superoxide dismutase (SOD) (Figure 3.2A). SOD activity in non-treated LIGHT$^{-/-}$ wounds was elevated by 4hr post-wounding and inhibition of GPx and catalase activity resulted in further increase in SOD activity compared to the C57BL/6 control wounds (Figure 3.2B/C). Consistent with this result, H_2O_2 levels were significantly elevated as early at 4hr post-wounding in the LIGHT$^{-/-}$ wounds, decreasing to control levels by 48hrs (Figure 3.2D). Furthermore, we observed that in LIGHT$^{-/-}$ mice, both GPx and catalase activities were similar to control mice, suggesting that accumulation of H_2O_2 was primarily caused by the inability of the antioxidant system to keep up with the oxidative stress.

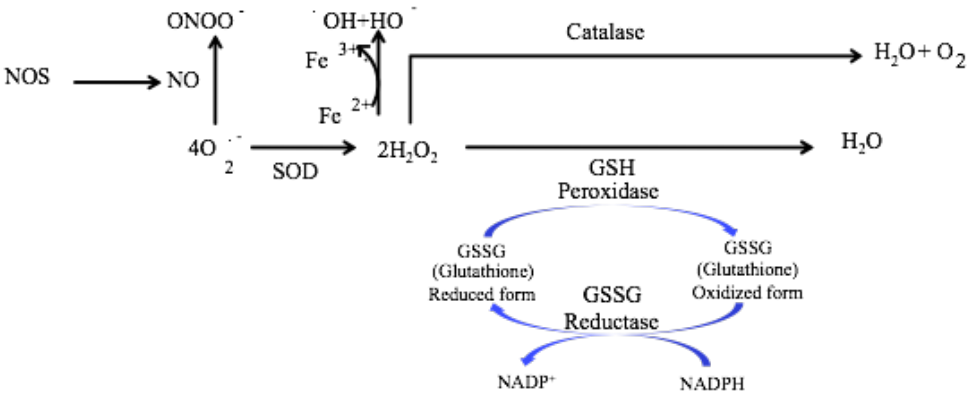

Figure 3.1. Schematic illustration of oxidative and nitrosative stress cycle. Superoxide dismutase (SOD) dismutates superoxide anions ($O2^{\cdot-}$) to generate H_2O_2. This reactive oxygen species (ROS) can be detoxified by catalase to H_2O+O_2 and by glutathione peroxidase (GPx) to H_2O. ROS can also enter the Fenton reaction in the presence of ferrous ions to give rise to $^{\cdot}OH+OH^{-\cdot}$ We also depict the $O2^{\cdot-}$ interaction with nitric oxide (NO) produced by nitric oxide synthetase (NOS) to give rise to peroxinitrite anion ($ONOO^{-}$). The effects of oxidative and nitrosative stress can cause lipid peroxidation, DNA damage, protein modification and cell death.

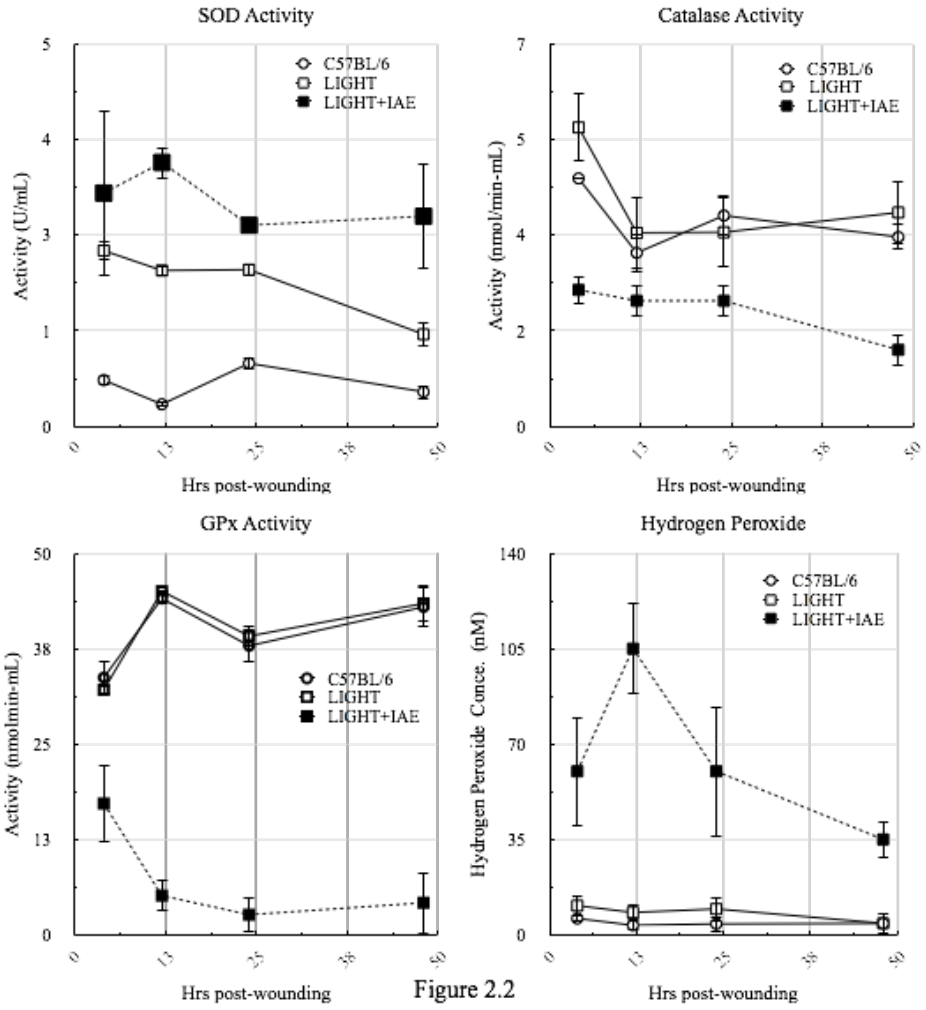

Figure 2.2

Figure 3.2: Oxidative stress is normally elevated in LIGHT$^{-/-}$ wounds and further increased with the use of IAE. (A) SOD activity was measured using a tetrazolium salt that converts into a formazan dye detectable at 450nm. SOD activity is significantly elevated in LIGHT$^{-/-}$ mice (□, solid line) in the first 48hrs post-wounding. SOD activity was further increased with IAE (■, dotted line). (B) Enzymatic reaction of catalase and methanol in the presence of H_2O_2 gives rise to formaldehyde, spectrophotometrically detected with purpald chromogen, at 540nm. Catalase activity in adult LIGHT$^{-/-}$ and control wounds was similar but significantly decreased with IAE. n=6. (C) GPx detoxifying activity was measured indirectly at 340nm by a coupled reaction with glutathione reductase where GPx activity was rate-limiting. The level of GPx activity in the adult LIGHT$^{-/-}$ wounds was essentially identical to that of the controls but significantly decreased with IAE. (D) Resofurin formation, detected at 590nm, was used to determine H_2O_2 levels. Significant increases in H_2O_2 very shortly post-wounding were seen and dramatically elevated with IAE. n=8.

Our previous findings (31) have indicated that high levels of ROS and the presence of biofilm-producing bacteria are the causative agents in turning acute or delayed healing wounds into chronic wounds. To test this hypothesis we significantly increased the oxidative stress in the wound with IAE and introduced the biofilm-producing bacteria, *S. epidermidis* C2, that we isolated from the spontaneously-developed chronic wounds of the LIGHT$^{-/-}$ mice (31). Treating the wound with IAE immediately after wounding and application of *S. epidermidis* C2 24hr later was sufficient to turn the wounds with impaired healing into chronic wounds 100% of the time and these remained open for > 4 weeks (Figure 3.3). Under the same conditions, the control C57BL/6 wounds closed in 15-19 days.

Bacterial infections are biofilm-producing and polymicrobic in LIGHT$^{-/-}$ chronic wounds. It has been established that bacteria that colonize chronic wounds in humans is often polymicrobic (many bacterial species) and biofilm-producing. To determine whether the LIGHT$^{-/-}$ chronic wounds also exhibited these phenotypes, we collected wound excretions (also called exudates) at varying time points and quantified biofilm production and composition of the bacteria that colonized the LIGHT$^{-/-}$ wounds. Staining of adherent bacterial mass with Hucker crystal violet has been widely used as readout for biofilm production (45, 112, 115, 116). We decided to quantify the ability of LIGHT$^{-/-}$ wound exudates (containing many bacterial species) and the individually isolated bacteria that composed these exudates for the production of adherent biofilms (Figure 3.4A). Biofilm quantification of wound exudates (which contain multiple bacterial species) demonstrated that the acute wound colonizing bacterial community, 5 days post-

wounding, is non-biofilm producing (OD570nm < 0.125). As expected, we found that coagulase-negative *Staphylococcus epidermidis* was present in the wounds throughout healing, given that we infected the wounds with *S. epidermidis* C2. However, co-colonizing bacteria were often isolated (Figure 3.4B). The co-colonizing bacterium isolated from day 5 exudate was identified as non-biofilm forming hemolytic *Streptococcus sp.* (Figure 3.4B/C). Earliest indication of wound exudates that contain biofilm-producing bacterial communities (OD570nm ≥ 0.125) was at 8 days post-wounding. This exudate is primarily made up of biofilm producing coagulase-negative *Staphylococcus* and oxidase positive Gram negative aerobic rods (presumptively *Pseudomonas sp.*) (Figure 3.4B/C). As the infection progresses, by day 16 post-wounding, the *Enterobacter cloacae* population dominates the wound with smaller populations of *S. epidermidis* and *Pseudomonas sp.* (Figure 3.4B). Irrespective of the shift in bacterial population of the wounds, the overall degree in biofilm production did not change significantly over time (Figure 3.4A). In addition, the degree of biofilm production from the individually isolated bacteria varies and is dependent on the time of isolation and is species specific (Figure 3.4C). By day 22 post-wounding, biofilm-producing *E. cloacae* dominated the wounds with traces of biofilm-producing *S. epidermidis*.

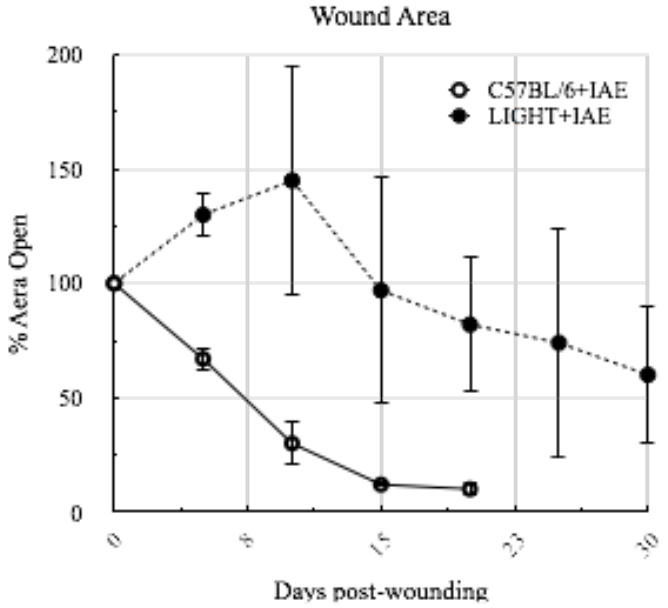

Figure 3.3: Manipulating redox parameters leads to development of LIGHT$^{-/-}$ chronic wounds. Wound areas were traced using ImageJ and % open wound area was calculated. The LIGHT$^{-/-}$ wounds remained open for a significantly longer time than the C57BL/6 wounds with similar treatment. n=8.

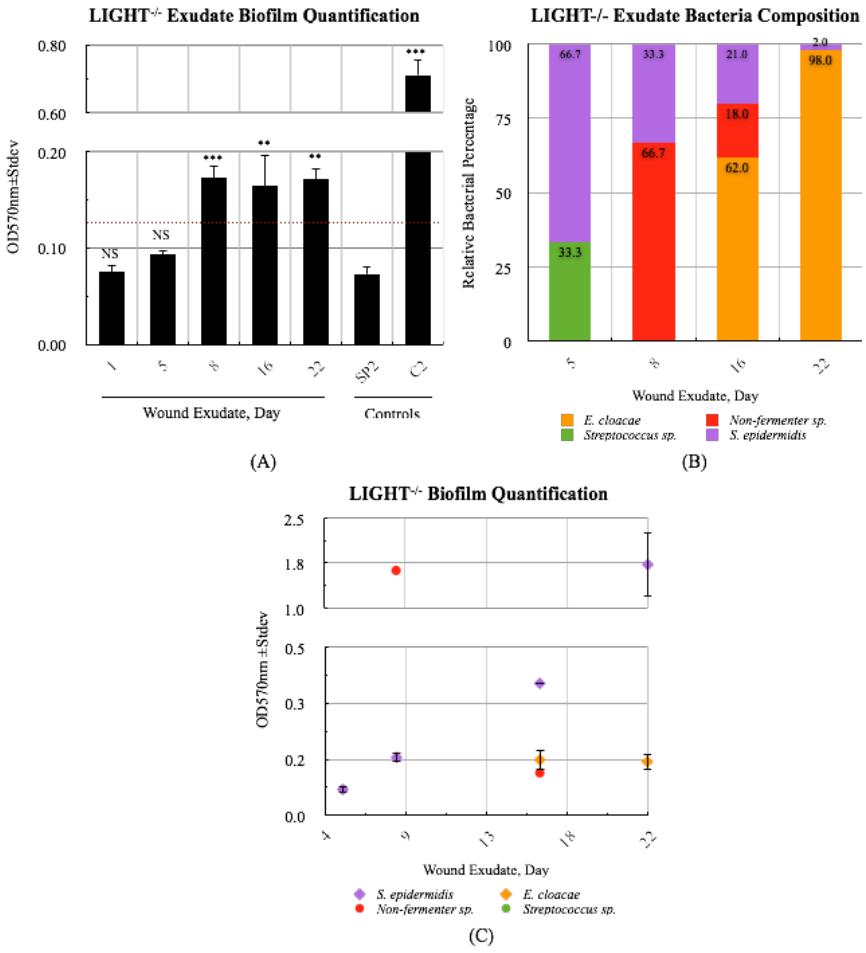

Figure 3.4: Identification and characterization of the bacteria that colonizes the LIGHT$^{-/-}$ chronic wounds. (A) Biofilm production was quantified by measuring the optical densities at 570nm of stained bacterial films adherent to plastic tissue culture plates. Biofilm quantitation of exudate (containing multiple bacterial species) obtained from wounds demonstrated that biofilm positive communities were observed by day 8 post-wounding and remained unchanged throughout. n=7. (B) Bacterial identification was carried out by growing bacteria on tryptic soy agar. Gram-negative rods were characterized using the API®20E identification kit. n= 7. The dynamics of the polymicrobic community in the wounds does not seem to affect the overall degree of biofilm production during the later stages of healing. (C) Individual contribution to biofilm production of bacteria isolated from wound exudates. Controls used to vindicate this assay were biofilm-negative (OD570nm < 0.125) *S. hominis* SP2 and biofilm-positive (OD570nm ≥ 0.125) *S. epidermidis* C2. n= 8.

To further confirm the presence of biofilm-forming bacteria in these wounds, we performed scanning electron microscopy on LIGHT$^{-/-}$ chronic wounds. An abundance of bacteria was observed in the wound and some of those bacteria were embedded in a biofilm-like matrix (Figure 3.5), with some of these appearing to reside in a defined niche surrounded by matrix. Beneath the biofilm we observed the presence of numerous inflammatory cells adherent to the extracellular matrix.

Bacterial burden and antibiotic resistance in LIGHT$^{-/-}$ chronic wounds. It has been reported that the majority of chronic wounds in humans have bacterial contamination and high levels of bacterial burden will likely result in impaired healing (26). At 5 and 8 days post-wounding, colony-forming unit counts (CFU/mL of exudate) from LIGHT$^{-/-}$ mouse exudates show low levels of bacterial burden ($1.6x10^3$ CFU/mL). However, these levels reach $4.0x10^7$ CFU/mL by day 22 post-wounding (Figure 3.6A).

It has been well established that biofilm-associated wound infections are extremely resistant to antimicrobial therapy (117, 118). To establish whether this is true for the bacterial community in LIGHT$^{-/-}$ wounds, we measured the community minimal inhibitory concentration (cMIC) of amoxicillin for these bacterial communities. The cMIC required to inhibit the growth of biofilm-producing bacterial community from LIGHT$^{-/-}$ wounds was determined to be 50μg/mL compared to the 0.4 - 0.8μg/mL required for non-biofilm producing colonizers (Figure 3.6B). This suggests that biofilm-producing bacterial communities isolated from LIGHT$^{-/-}$ chronic wounds are ~50X more resistant to killing by amoxicillin compared to their non-biofilm producing counterparts.

Secondary bacterial infections in LIGHT$^{-/-}$ wounds are likely to originate from the animal skin microbiome. In order to determine whether the skin of mice contains the bacteria that eventually make biofilms in the chronic wounds, we took skin swabs from unwounded LIGHT$^{-/-}$ mice and cultured them *in vitro* (Figure 3.6C). The majority of the cultured bacteria belong to the Firmicutes phylum, specifically *Staphylococcus spp*. and *Streptococcus spp*. We also documented the presence of bacteria that belong to the Proteobacteria phylum (e.g., various Gram-negative rods and *E. cloacae*). These bacteria are all known to be associated with the human skin microbiota (119).

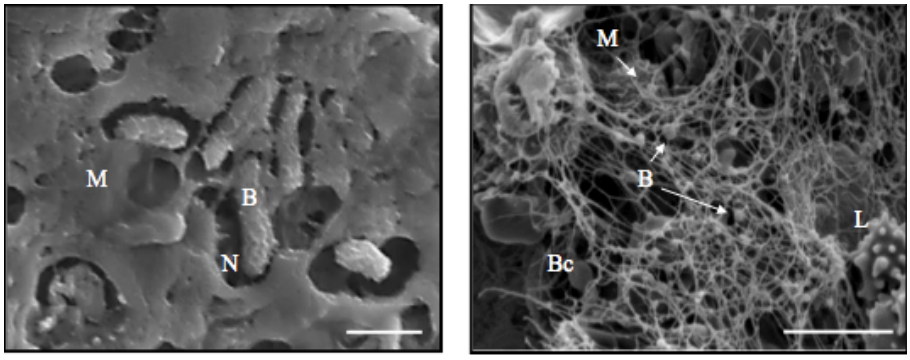

Figure 3.5: Scanning electron microscopy characterization of biofilm present in LIGHT$^{-/-}$ wounds. Scanning electron microscopy (SEM) images of the Au/Pd sputtered, fixed and dried, chronic wound samples were captured using an XL30 FEG SEM. (A) Image shows the presence of bacterial rods [B] in the wound bed. (B) High magnification image of bacteria embedded in a biofilm- associated matrix [M] in a well defined niche [N]. Matrix beneath the biofilm show the presence of matrix and of coccal-shaped bacteria. A lymphocyte [L] and red blood cell [Bc] were highlighted for size references. Scale bars 1μm (A) and 5μm (B).

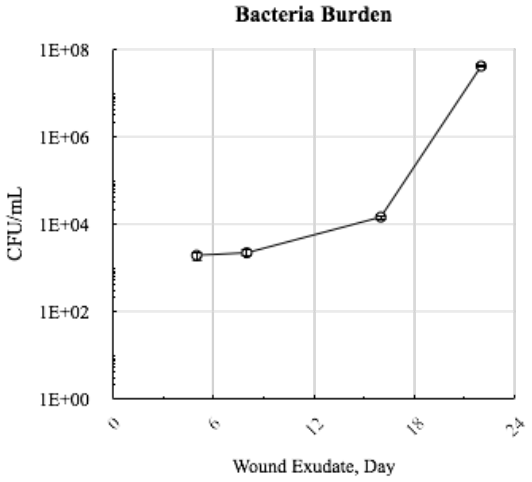

(A)

Amoxicillin cMIC	
Exudate	Conc'
Day 5	0.4-.0.8µg/mL
Day 22	50µg/mL

(B)

LIGHT$^{-/-}$ Skin Microbiota	
Firmicutes	Proteobacteria
• Coagulase-negative *Staphylococcus sp.* • *Streptococcus spp.*	• *Enterobacter cloacae* • Oxidase positive Gram negative aerobic rods

(C)

Figure 3.6: LIGHT$^{-/-}$ wounds bacterial burden, antibiotic sensitivity, and skin microbiota. (A) Bacterial burden was evaluated by colony forming unit count. The CFU/mL were relatively low during the early phases of healing and were highest during the impaired and chronic stages of healing. n= 7. (B) Antibiotic challenge on wound exudates collected from LIGHT$^{-/-}$ mice was done using Amoxicillin. The cMIC of amoxicillin on the bacteria found in the chronic LIGHT$^{-/-}$ wound exudate at day 22 was 50µg/ml, much higher than exudate collected at day 5 when biofilm is not yet abundant. (C) Normal skin swabs were collected from LIGHT and C57BL/6 mice to evaluate resident organisms. The microbiota of the skin was similar in both control (C57BL/6) and LIGHT$^{-/-}$ mice.

Wound chronicity is achieved by inhibiting GPx and catalase enzymes in db/db mouse model. We recently demonstrated that increased oxidative stress and the presence of biofilm-producing bacterial infection set the wound on a course toward chronicity in the LIGHT$^{-/-}$ animal model. Given our observations, we decided to test whether wound chronicity can be achieved using a more clinically relevant animal model with the same conditions used to generate the LIGHT$^{-/-}$ chronic wounds. Since diabetic patients have higher risks in developing chronic wounds (e.g., foot ulcers), using the type II diabetic (*db/db)* mouse model of delayed wound healing we further increased oxidative stress in the *db/db* wounds with IAE at the time of wounding and observed whether these wounds would become chronic. We observed that a single regimen of IAE was sufficient to turn *db/db* acute wounds into chronic wounds (Figure 3.7). These wounds usually remained open for >70 days. C57BL/6 control wounds treated with the same regimen remained open for only 19 days.

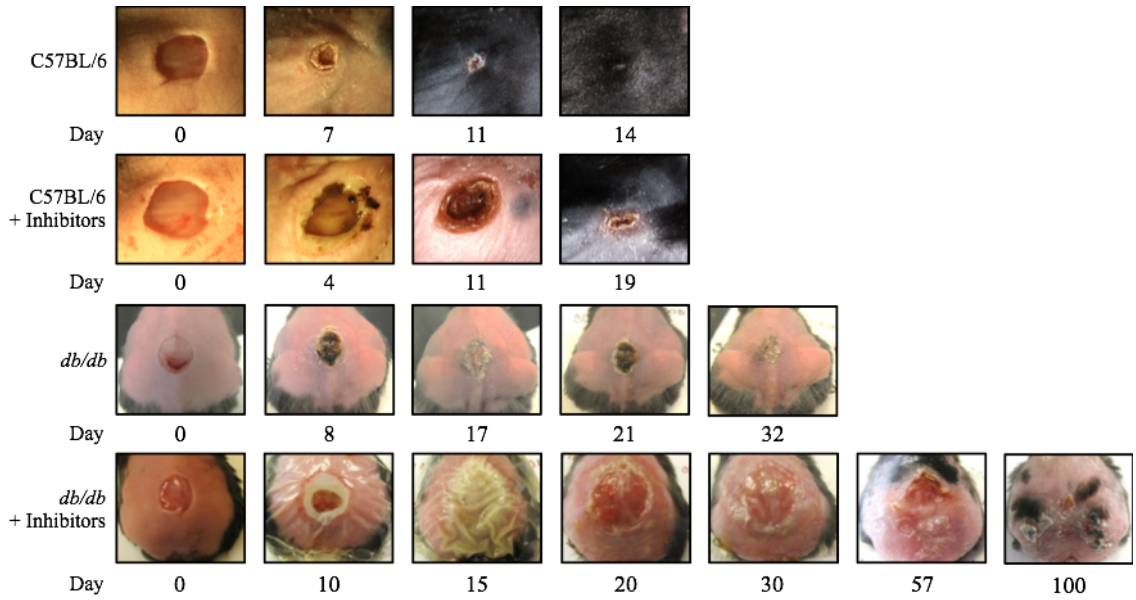

Figure 3.7: Images of wounds from db/db and control mice. The pathophysiological progression of control (C57BL/6), *db/db* non-treated, and *db/db* treated wounds after a single treatment of IAE. After 14 days post wounding, the control mouse wound healed with no sign of infection. Untreated db/db mice exhibit a delayed wound healing phenotype and took 32 days to heal after wounding. In contrast, the IAE treated *db/db* wounds showed signs of infection by the production of oozing exudates that contain bacteria, and remained open for >70 days.

Db/db wounds sustain spontaneous and complex bacterial infections. Like human wounds that become chronic, *db/db* wounds acquire spontaneous multiple species bacterial infections and become chronic with biofilm-producing bacteria. Analyzing wound exudates from *db/db* mice at various time points, we documented that bacterial infection was observed as early as 4 days post-wounding and persisted for at least 60 days in most animals (Figure 3.8). The presence of biofilm-associated bacterial infection in wound exudate was first seen around 16 days post-wounding (Figure 3.8A). Bacterial isolation and characterization showed that *db/db* wound exudates are comprised of many bacterial species (Figure 3.8B/C). Identifying and quantifying these bacterial species, we demonstrated that *S. epidermidis* and *Neisseria sp.* populations dominated the wound during the acute phase (4 days post-wounding, 25% and 50%, respectively) with lesser populations of *Pseudomonas sp.* (13%) and *E. cloacae* (13%). Interestingly, biofilm quantitation of individual bacterial species revealed that *S. epidermidis* isolated from day 4 produces biofilm when grown independently from the community (Figure 3.8B), suggesting that communal interactions may be an important regulator of biofilm production. As the infection progresses, the bacterial composition evolves from several species of non-biofilm producers (day 4) to a bacterial community that is composed of both biofilm and non-biofilm producing bacterial species. Earliest biofilm positive exudates were found in day 16-18 composed of biofilm-producing *S. epidermidis* (22%) and *Enterococcus sp.* (71%) and non-biofilm producing *Pseudomonas sp.* (2%) and *E. cloacae* (5%). As the wounds progress to a chronic phase (day 26 post-wounding) the bacterial profile has shifted and is predominated by biofilm producing *Enterococcus sp.*

(59%) and non-biofilm producing *E. cloacae* (33%) with traces of biofilm-producing *Pseudomonas sp.* (6%) and *S. epidermidis* (2%). By day 56 post-wounding, the wounds have transitioned from a polymicrobic infection profile to a monospecies infection by biofilm-producing *E. cloacae*. It has to be pointed out that *E. cloacae* was initially a non-biofilm producer but acquired the biofilm-producing phenotype during the latter stages of infections.

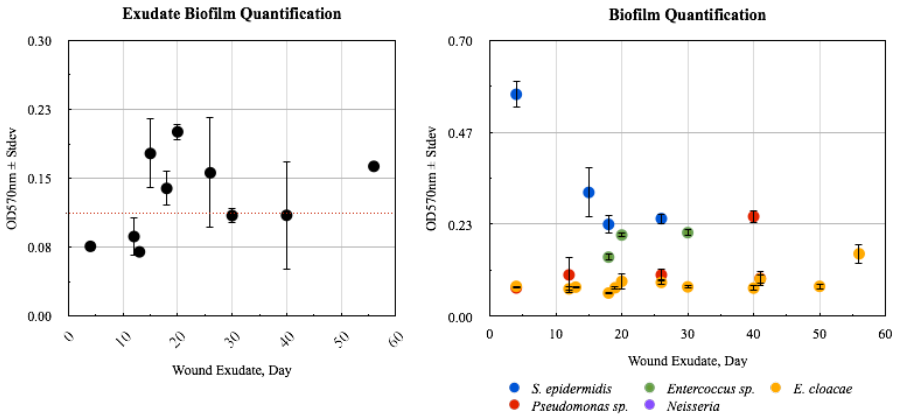

(A) (B)

Bacterial Prevalence (% Biomass)				
	Day4	Day18	Day26	Day56
S. epidermidis	25%	22%	2%	ND
Enterococcus sp.	ND	71%	59%	ND
Neisseria sp.	50%	ND	ND	ND
Pseudomonas sp.	13%	2%	6%	ND
E. cloacae	13%	5%	33%	100%
Total CFU/mL	$5.2x10^6$	$6.7x10^7$	$7.9x10^7$	$3.5x10^7$

(C)

Figure 3.8: Profile of the bacteria that colonized db/db wounds. (A) Wound exudates were quantified for biofilm production by measuring the optical densities of stained adherent bacterial films at OD570nm. (OD570nm $\geq$ 0.125 is considered to be biofilm positive). (B) Individual bacterial colony biofilm-forming-capacity was measured by measuring the optical densities of extracellular polysaccharide substance deposited on flat-bottom tissue culture plates. (C) Bacterial prevalence of individual species shows the changing dynamics of the wound microbiota. Wound infection is initially polymicrobic and progressively advances toward a monospecies infection dominated by biofilm-producing *E. cloacae*.

Db/db wounds sustain high bacterial burden. Impaired healing has been shown to be associated with high bacterial burden (26). CFU counts from wound exudates revealed that bacterial burden was at its highest around day 18-26 post-wounding ($6.7\text{-}7.9 \times 10^7$ CFU/mL), thereby pushing the wound into a state of chronicity. At day 30, there was a reproducible dramatic decrease in bacterial burden compared to day 20 (data not shown) that coincided with the disappearance of *S. epidermidis* and of *Pseudomonas sp*. However, by day 56, the wound bioburden was dominated by *E cloacae*, had recovered to a level comparable to day 20, and remained relatively high and unchanged thereafter (Figure 3.8C).

Chronic wound microbiota are resistant to antibiotic challenge. Bacterial communities living within biofilms are often resistant to antibiotics (117). Quantifying the bacterial cMIC of amoxicillin, carbenicillin, and gentamicin required to inhibit the growth of the bacterial community demonstrated that biofilm-positive bacterial communities (appearing >16 days) are more resistant to antibiotic killing, and this resistance increased with time (Table 3.1). Biofilm negative bacterial communities collected at 4 and 12 days post-wounding showed a cMIC ranging from 3-13μg/ml for all tested antibiotics. By day 26, when the wounds have become frankly chronic and contain biofilm, the cMIC was observed to be 50-100μg/ml for all tested antibiotics. By 56 days cMIC was determined to be 100μg/ml for gentamicin and well above 100μg/ml concentration for amoxicillin and carbenicillin. This dramatic increase in cMIC is strongly associated with the biofilm-producing phenotype.

Community Minimal Inhibitory Concentrations			
Wound Exudate	Amoxicillin (μg/mL)	Carbenicillin (μg/mL)	Gentamicin (μg/mL)
Day4	6	6	3
Day12	6	13	6
Day26	50-100	100	50
Day56	>100	>100	100

Table 3.1: Biofilm-associated bacterial infections in db/db chronic wounds are insensitive to antibiotics. The community Minimum Inhibitory Concentration (cMIC) on wound exudates was examined using the antibiotics amoxicillin, carbenicillin, and gentamicin. Wound exudates collected from the chronic phase (day 26 and 56, biofilm positive) were found to be significantly more resistant to antibiotic challenge compared to exudates collected at day 4 and 12 when biofilm is not yet abundant.

Treatment with antioxidant agents affects biofilm production and bacterial burden resulting in a better wound healing phenotype. Given that increased ROS stress resulted in the production of chronic wounds with sustained biofilm-associated bacteria in the *db/db* model, we asked whether abating ROS stress during chronicity would help the wound to heal. Given that the wounds are chronic by 20 days post-wounding and bacterial burdens are at its highest, we treated the animals on day 20 post-wounding with two antioxidant agents (AOA), N-acetyl cysteine (NAC) and α-tocopherol, and observed the wounds for more than 30 days post-AOA treatments. NAC is the prodrug of L-cysteine, which is a precursor to the biologic antioxidant glutathione (120). α-Tocopherol is a lipid-soluble compound and is the most active form of vitamin E, best known for its antioxidant function (121-123). We found that the healing improved dramatically by 30 days post-AOA treatment compared to wounds not treated with AOA. Non AOA-treated wounds often take up to 100 days to close (Figure 3.9). After 10 days post-AOA treatment (day 30 post-wounding), the biofilm-producing capacity of the chronic wound bacterial community is reduced by ~30% (Figure 3.10A). By day 50 post-wounding the bacterial community was considered to be negative for biofilm production (OD570nm < 0.125). CFU counts (Figure 3.10B) revealed a marked decrease in bacterial burden at 10 days of AOA treatment that, in contrast to non-AOA-treated wounds, remained relatively unchanged thereafter.

To determine whether the reduction in biofilm production resulting from AOA treatment enhances the antimicrobial effect of amoxicillin, cMICs of wounds treated with NAC and α- tocopherol were evaluated (Table 3.2). After 10 days of antioxidant

treatment, the cMIC for amoxicillin was reduced approximately two-fold. Prolonged treatments with AOA (30 days of antioxidant treatment) resulted in antibiotic sensitivity levels comparable to non-biofilm producing bacteria isolated from the acute stage of infection. Similar results were observed with other antibiotics such as carbenicillin and gentamicin (Table 3.2). These observations confirm that abating redox stress with AOA alters the wound environment resulting in a bacterial phenotype that produces less biofilm and is more sensitive to antibiotics.

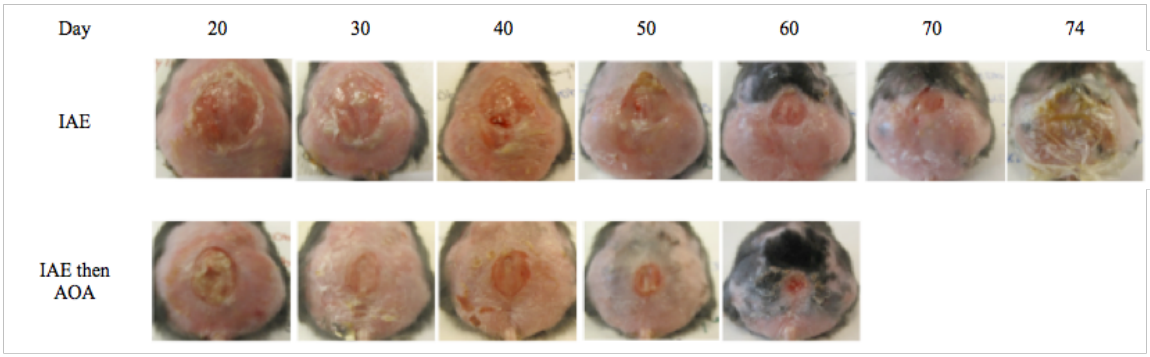

Figure 3.9 Chronic wounds treated with AOA leads to better healing. Chronic wounds of *db/db* mice treated with IAE (immediately after wounding) and then AOA (at day 20), show a faster rate of wound closure compared to IAE only treated wounds.

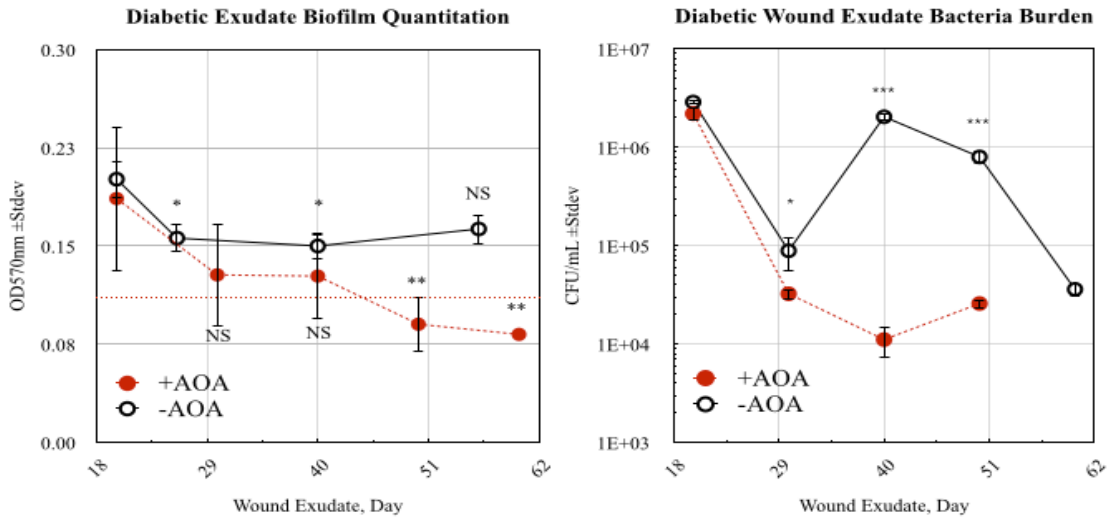

(A) (B)

Figure 3.10: AOA treatment reduces biofilm-forming bacteria and increases bacterial antibiotic susceptibility. (A) Wound exudates' biofilm production was evaluated by measuring optical densities at OD570nm. AOA treatment (administered at day 20 post wounding) reduced biofilm formation when compared to pre-AOA treatment. (B) Bacterial burden measured by colony forming unit counts was significantly reduced in AOA-treated (NAC/αToc) *db/db* wounds.

Community Minimal Inhibitory Concentrations			
Wound Exudate	Amoxicillin (μg/mL)	Carbenicillin (μg/mL)	Gentamicin (μg/mL)
Day20	25	25-50	13-25
Day30	13-25	13	3-6
Day40	6-13	6-13	3-6
Day50	6	6	3-6

Table 3.2 Community minimum inhibitory concentrations. cMIC of bacteria present in wounds treated with AOA was performed using Gentamicin (Gm), Carbenicillin (Cb), and Amoxicillin (Amox). cMIC for non-AOA treated controls are shown on Table 3.1.

Discussion

We have shown that we can create chronic wounds by manipulation of the impaired wounds of LIGHT$^{-/-}$ mice using antioxidant enzyme inhibitors and by adding biofilm-forming bacteria previously isolated from the naturally occurring chronic wounds of these transgenic mice. This approach leads to the generation of chronic wounds 100% of the time. We also demonstrated that wound chronicity can be generated in a diabetic (*db/db*) mouse model of impaired healing by increasing the levels of oxidative stress in the wound tissue. These wounds remain chronic up to >70 days post-wounding. Both the LIGHT$^{-/-}$ and *db/db* wounds are characterized by: [1] presence of a polymicrobic bacterial infection, [2] sustained high levels of bacterial burden, [3] biofilm-producing bacteria, and [4] biofilm-producing bacterial species insensitive to antibiotics. Furthermore, we demonstrated that chronicity of *db/db* wounds can be reversed by application of appropriate AOA, leading to proper healing.

Chronic wounds and difficult-to-heal wounds are postulated to have an underlying biofilm-associated bacterial contribution that is polymicrobic and dynamic (2, 26, 36, 124). We show that chronicity in LIGHT$^{-/-}$ and *db/db* wounds is accompanied by a persistent bacterial infection that is composed of many bacterial species and contains both non-biofilm and biofilm-producing bacteria. Furthermore, we showed that the source of infection arises from the LIGHT$^{-/-}$ and *db/db* mouse skin microbiota. Similar observations have been documented for human chronic wounds (125, 126).

Staphylococcus epidermidis and other coagulase-negative staphylococci exist as harmless or even beneficial commensal bacteria of the human's skin. However, in

diabetic, elderly, and immobile individuals, these commensal bacteria can cause diseases and are responsible for a large percentage of infection in wounds that do not heal (127). The contribution of *E. cloacae* in nosocomial infections are well known (128); however, much less is known about *E. cloacae* infection in chronic wounds, although its presence is often reported (129) in diabetic foot infection (130, 131), diabetic gangrene (132), and chronic venous leg ulcers (42, 133).

In our animal models, bacteria that colonize the LIGHT$^{-/-}$ *db/db* mouse wounds are often identified as *S. epidermidis*, *Enterococcus sp.*, *Enterobacter cloacae*, and *Pseudomonas sp.* These bacterial species exist as a dynamic community and differ largely by the time of isolation and relative abundance in both animal models. Although commensal gram-negative bacteria *E. cloacae* are not reported from normal human skin, their presence in human wounds comes from gastrointestinally contaminated skin (127, 134). Perhaps the lack of consideration of *E. cloacae* contribution to the development of chronic wounds may be in part due to their relatively lower initial abundance compared to the more commonly isolated bacteria such as *Staphylococcus spp.*, *Enterococcus spp.*, and *Pseudomonas aeruginosa* (26, 42, 135).

Others have shown that bacteria cultured from patients with venous leg ulcers with or without clinical symptoms are polymicrobic (42, 133). Furthermore, similar microbiota are found in combat wounds, chronic necrotizing skin diseases, and other chronic wounds (136-138). These studies show the diversity and dynamism of wound bacteria and their ability to produce biofilm changes over time with establishment of selective bacterial populations. These attributes are probably due to both bacterial

competition and cooperation in concert with the unique clinical phenotype and pathophysiology of the host wound tissue. In the diabetic mice of our study, chronic wounds evolve into essentially a monospecific infection dominated by biofilm-producing *E. cloacae*. In other species (including humans), the specific biofilm producers may differ but the overall result is likely to be the same.

We find that an overall buildup of ROS increased oxidative stress very early in the wound microenvironment and also that AOA treatment significantly increased both catalase and GPx activity, two critical enzymes that decrease oxidative stress. Furthermore, biofilm is no longer observed in the AOA-treated wounds, suggesting that redox balance can modulate biofilm production by the colonizing bacterial community, resulting in significant improvement in wound healing. Therefore, the critical factors in human chronic wounds are the presence of oxidative stress coupled with the presence of bacterial biofilms.

CHAPTER 4

Norspermidine increases the bactericidal effect of gentamicin in biofilm-positive bacteria that colonize mouse chronic wounds

Abstract

Biofilms are communities of bacteria living within an extracellular polysaccharide matrix. Norspermidine has been shown to decrease the adherence of bacterial biofilms from *S. aureus* and *E. coli, in vitro*. However, this effect has not yet been documented for biofilm-associated bacterial infection that is composed of many species, like those found in chronic wounds. Using chronic wounds generated in our diabetic (*db/db*) mouse model, we show that biofilm positive bacterial communities are insensitive to antibiotic killing compared to its non-biofilm producing counterparts. Furthermore, we demonstrated that application of norspermidine decreases the amount of adherent biofilms produced by these colonizing bacterial communities and increases the bactericidal effect of gentamicin. Given its effect on multiple bacterial species, we believe that norspermidine could be used in combination with bactericidal antibiotics to control biofilm-associated bacterial infection in dermal chronic wounds.

Introduction

Biofilms are a community of sessile bacteria living within a self-produced extracellular polysaccharide (EPS) matrix. Nearly all bacteria found in nature have the capacity to produce biofilms (139). Bacterial biofilms are found in chronic wounds and wounds that are difficult to heal. They contribute to both the infection of the wounds and their inability to heal (140). Chronic wound management costs the United States ~$25 billion annually (33). Bacteria in biofilms are insensitive to antimicrobial agents (117) and bacterial biofilm-associated infections are not resolved by the host immune system (141). This is largely due to the lack of antibiotic penetration and the inactivation of the antimicrobial agents by the anionic polysaccharide barrier (2, 142), the inability of immune cells to phagocytose bacteria in biofilms, and the ability of the biofilms to block complement activation and phagocyte chemotaxis (143, 144). Therefore, biofilm-related infections are extremely problematic and difficult to treat.

Although numerous models have been developed to study the underlying cause of chronic wounds, the lack of animal models that resemble human chronic wound pathophysiology has made it difficult to evaluate new wound healing therapies (27-30). Our group demonstrated that by inhibiting specific key redox systems, we were able to generate chronic wounds in the type II diabetic mouse model (*db/db*) with spontaneous chronic biofilm-associated bacterial infections (see chapter 3). Furthermore, the source of the infection likely originates from the animal skin microbiome. This pathogenicity is similar to that of human chronic wounds.

It has been previously shown that before *Bacillus subtilis* biofilms are disassembled, the bacteria produced a factor that causes the release of amyloid fibers that linked the cells in the biofilm (46). This factor was shown to be a mixture of D-amino acids. *In vitro*, it was also shown that D-amino acids block the subsequent growth of the biofilm-associated bacterial community of *Staphylococcus aureus* but had little effect on EPS matrix production and localization (145). More recently, it has been shown that the polyamine, norspermidine, causes the disruption of adherent biofilms produced by *Escherichia coli* and *Staphylococcus aureus in vitro* (45). Unlike D-amino acids, norspermidine is thought to interact with the EPS matrix causing the collapse of the biofilms (45). To our knowledge, the ability of norspermidine to disrupt biofilms has not yet been evaluated for bacterial biofilms associated with chronic wounds. Given the non-specificity of norspermidine, it is conceivable that norspermidine may be able to disassemble biofilms produced by bacteria that are found in chronic wounds.

Using the exudates collected from our generated *db/db* chronic wounds that contain bacteria from the wounds, we identified the bacterial species that colonized the wound at varying time points; we then evaluated whether norspermidine can disrupt adherent biofilms produced by these bacteria, rendering them more sensitive to the bactericidal activity of antibiotics.

Materials and Methods

Materials and Reagents: Tryptic soy broth (TSB) and Tryptic soy agar (TSA) were purchased from Difco (Sparks, MD). Norspermidine (Bis(3-aminopropyl)amine), amoxicillin and carbenicillin were purchased from Sigma-Aldrich (St. Louis, MO) and gentamicin was purchased from Biosynth (Itasca, IL). Defibrinated sheep blood was purchased from ColoradoSerum Company (Denver, CO) and Congo red dye from Sigma-Aldrich. Mercaptosuccinic acid and 3-amino-1,2,4-triazole were from Sigma Lifescience (St.Louis, MO), and 0.22µm polyethersulfone membrane was from EMD (Billerica, MA). Optical density was quantified using a SpectraMax M2e microplate reader from Molecular Device (Sunnyvale, CA) or an iMark Microplate Absorbance Reader 168-1130 from BioRad (Hercules, CA). Gram-stained slides were visualized using a Carl Zeiss 47-30-11-9901 microscope (Thornwood, NY).

Diabetic (db/db) dermal excisional chronic wound model: The creation of chronic wounds was carried out using 6-7 month-old *db/db* mice (homozygous for the diabetes spontaneous mutation $Lepr^{db}$) purchased from the Jackson laboratory (Bar Harbor, ME). The midline hairs on the back of the mouse were removed using Nair Hair Remover 24hr prior to wounding. A single full-thickness wound (excision of the skin and the underlying panniculus carnosus) was made using a 7mm biopsy punch. Db/db chronic wounds were induced by inhibiting the catalase and peroxidase antioxidant systems. Catalase activity was inhibited by 3-amino-1,2,4-triazole via intraperitoneal injection at a concentration of 1g/kg body weight 20min prior to creating the excisional wound, and glutathione peroxidase activity inhibition was done by using mercaptosuccinic acid topically at a

concentration of 150mg/kg body weight immediately after wounding. The wound was immediately covered with sterile Tegaderm (3M, St. Paul, MN). Similar treatment was carried out using age-matched C57BL/6 mice. All animals were housed at the University of California, Riverside vivarium and all experimental protocols were approved by the UCR Institutional Animal Care and Use Committee.

Bacterial culture and identification: From a single generated *db/db* chronic wound, wound secretion, also called exudate, containing bacteria was collected by swabbing the wound with a sterile cotton swab. The swabs were then placed in sterile 1% w/v protease-peptone and 10% v/v glycerol, vortexed, and stored at -80^{o}C. Prior to use, exudates were ice thawed and bacteria were serially diluted in TSB before being cultured on TSA plates containing 3.0% v/v defibrinated sheep blood and 0.08% w/v Congo red dye for 16-18hr at 37^{o}C in a humidified incubator. All cultured bacterial colonies were initially differentiated based on colony size, texture, hemolytic pattern, and Congo red dye uptake. The colonies were isolated, examined for Gram stain reactivity, and visualized using a Carl Zeiss 47-30-11-9901 light microscope. The API$^{®}$20E identification kit, growth on *Pseudomonas* Isolation Agar, oxidase test, and motility assay were used to identify Gram-negative rods. Gram-positive cocci were differentiated based on catalase activity, coagulase activity, and hemolytic activity. Biofilm positive coagulase-negative *Staphylococcus* C2 strain was previously isolated from TNFSF14/LIGHT$^{-/-}$ mouse chronic wounds (31) and used as positive control and biofilm negative *Staphylococcus hominis* SP-2 was purchased from ATCC (cat#35982, Manassas, VA) as negative control.

Biofilm-formation quantitation: Adherent biofilms were quantified using a previously described method (112) with minor modifications. Briefly, 5μL of exudate (collected from a wound that contains many bacterial species) or 3μL single bacterial species (isolated from the wound exudate) was seeded and grown stationary in TSB in a humidified incubator at 37^{o}C on a sterile 96-well polystyrene flat-bottomed tissue culture plate. After incubation, the bacteria were removed by tipping the plate over and gently flicking the plate. The wells were washed three times with tap water by slowly submerging the plate and then flicking to remove the water. This ensures that non-adherent bacteria were properly removed. The wells were dried by tapping on absorbent paper and then air dried at 65^{o}C for 30min. The plate was then cooled to room temperature and stained with Hucker crystal violet (146) for 5min. Excessive stain was removed by rinsing the plate with tap water and then air dried overnight. The optical density at 570nm of adherent bacteria and biofilms was taken using the SpectraMax M2e microplate reader (Molecular Device, Sunnyvale, CA). $OD_{570nm} \geq 0.125$ was deemed biofilm positive as previously described (112).

Bacterial community minimal inhibitory concentration*:* Amoxicillin, carbenicillin, and gentamicin antibiotic solutions were prepared as instructed by manufacturers and sterile filtered through a 0.22μm polyethersulfone membrane. Bacterial community or single bacterial species were seeded using 5μL of wound exudate (contains a mix of bacterial species) or individually isolated bacteria (from a particular wound exudate) in a total volume of 75μL of TSB into a flat-bottomed 96-well polystyrene tissue culture plate (in triplicate) and incubated at 37^{o}C for 3-4hr in a humidified incubator. This step allows the

bacteria adequate amount of time to recover and adhere to the polystyrene tissue culture plate. Bacteria were challenged with varying concentrations of amoxicillin, carbenicillin, or gentamicin in a total volume of 150µL of TSB for 12hr at 37°C. The OD_{595nm} was quantified using the iMark Microplate Absorbance Reader 168-1130 (BioRad, Hercules, CA) immediately after the addition of antibiotics and after the 12hr incubation period. After 12h of incubation in a humidified incubator at 37°C, we define the community Minimal Inhibitory Concentration (cMIC) as the lowest antibiotic concentration that resulted in a ≤1.5X (≤50% increase) change in the optical density measured at 595nm (ΔOD_{595nm}) after 12hr of incubation compared to the OD_{595nm} immediately prior to the introduction of antibiotic.

Norspermidine assay: Bis(3-aminopropyl)amine, also known as norspermidine, was prepared for assay as directed by the manufacturer. To evaluate the effect of norspermidine on biofilms, 5µL exudates from 26 or 56 days post-wounding were seeded in a volume of 75µL of TSB in a flat-bottomed 96-well plate and incubated for 4-6hr at 37°C in a humidified incubator. After incubation, the cells were treated with increasing concentrations of norspermidine for 12hr. The OD_{595nm} was taken immediately after the norspermidine introduction and then after 12hr of incubation to monitor bacterial growth. Adherent biofilms were quantified as previously described. To evaluate the bactericidal effect of gentamicin, cells were seeded (as described above) and then grown with or without 2mM of norspermidine for 12hr before challenged with gentamicin at 100µg/mL for 2-2.5h at 37°C. Viable cells were quantified as described below.

To determine whether norspermidine has affected biofilm production permanently, 5µL of day 26 and day 56 post-wounding exudate or the control bacteria, *S. epidermidis* C2 and *S. hominis* SP2, were seeded on 96-well plate in 150µL TSB containing 2mM of norspermidine for 12hr at 37^{o}C. After the incubation period, the bacteria were removed, washed with sterile saline, and seeded in fresh TSB without norspermidine for another 12hr at 37^{o}C. Biofilm formation was then quantified as described previously.

Viable cell count: Bacterial cultures/samples were first diluted 1:4 v/v with TSB and then serially two-fold diluted in a flat-bottomed 96-well polystyrene tissue culture plate. A 25µL aliquot of each dilution was plated onto TSA plates containing 3% v/v sheep red blood cells and incubated at 37^{o}C overnight in a humidified incubator. Colonies were counted visually.

Statistical analysis. All data are expressed as the mean average of at least three independent replicates ± standard deviation (StDev). A two-tailed Student's *t*-test was used to compare values obtained from two independent groups. p-Values ≤0.05 were considered statistically significant. Statistical comparisons were reported as p-Value ≤ 0.05 (*), p-Value ≤ 0.01 (**), and p-Value ≤ 0.001(***); NS = not significant.

Results

Biofilm positive bacterial communities isolated from chronic db/db wounds are complex and resistant to amoxicillin, carbenicillin, and gentamicin killing. Bacteria cultured from acute (≤18 days post-wounding) and chronic (≥26 days post-wounding) wound exudates demonstrated that *db/db* wounds are largely infected with a community of bacteria that are made up of many species. Quantifying the production of adherent biofilms (112) demonstrated that the bacterial communities cultured from chronic wound exudates (day 26 and day 56 time points) are positive for biofilm production (Figure 4.1A). Individual bacterial species isolated from day 26 exudates show that they contain both biofilm-producing ($OD_{570nm} \geq 0.125$) and non-biofilm ($OD_{570nm} < 0.125$) producing species. These biofilm-producing bacteria are identified as coagulase-negative *Staphylococcus* and hemolytic *Enterobacter sp.* Non-biofilm producing species are determined as *Pseudomonas sp.* and *Enterobacter cloacae*. Interestingly, at the latter stage of chronicity (day 56 time point), the wounds have transitioned from many bacterial species infection to a single species infection (Figure 4.1B). This dominant bacterium is identified as biofilm-producing *E. cloacae*. It is important to point out that *E. cloacae* has acquired the biofilm-producing phenotype, whereas it was previously isolated as a non-biofilm producing bacterium (Figure 4.1B).

To establish whether the bacterial communities contained in the wound exudates and individual biofilm-producing species (isolated from a particular wound exudate) that colonize *db/db* wounds are resistant to antibiotic killing, the cMICs (described in Materials and Methods) were determined for two β-lactam antibiotics (amoxicillin and

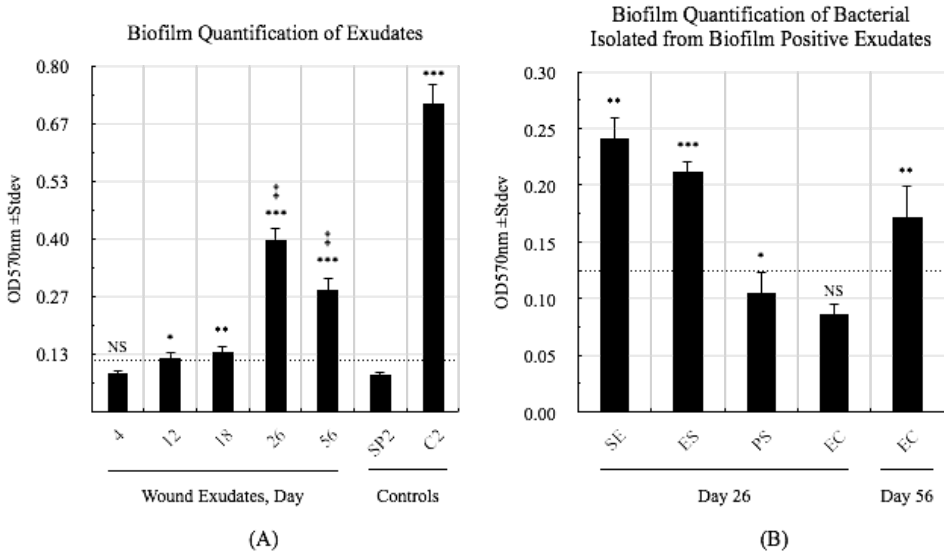

Figure 4.1: Quantitation of adherent biofilms. (A) Wound exudates, containing many bacteria that infected the wounds, were cultured and stained for adherent biofilms. Biofilm was quantified by measuring the optical density of adherent bacteria and EPS matrix stained with Hucker's crystal violet (see Materials and Methods). $OD_{570nm} \geq 0.125$ was considered to be biofilm positive. The biofilm negative *S. hominis* SP2 (147) and biofilm positive *S. epidermidis* C2 (31) were used as controls. Dotted line indicates biofilm positive (above) or biofilm negative (below) bacteria. Definition adopted from Christensen et al. (112). (‡) Indicate chronic wounds. (B) Biofilm quantification of individual bacterial species isolated from biofilm positive exudates. SE: coagulase-negative *Staphylococcus* (presumptively *S. epidermidis*), ES: *Enterococcus sp.*, PS: *Pseudomonas sp.*, and EC: *Enterobacter cloacae*.

carbenicillin) and an aminoglycoside (gentamicin). The cMIC of amoxicillin, carbenicillin, and gentamicin for the exudate bacterial community isolated at day4 post-wounding was determined to be 6μg/mL, 6μg/mL, and 3μg/mL, respectively (Table 4.1). This exudate bacterial community is made up of coagulase-negative *Staphylococcus*, *Enterobacter cloacae*, Gram-negative catalase-positive cocci (presumptively *Neisseria sp*.), and *Pseudomonas sp*. (Table 4.2) and together they are determined to be non-biofilm producing. A two-fold increase in the cMIC for carbenicillin (13 μg/mL) and gentamicin (6μg/mL) were observed for day 12 and 18 exudate bacterial communities compared to day 4. No cMIC change was observed for amoxicillin. Earliest detection of a biofilm-positive bacteria community was observed from wound exudate collected day 26 post-wounding (figure 4.1A). The cMIC was determined to be at 100μg/mL for amoxicillin and gentamicin and 50μg/mL for carbenicillin (Table 4.1). This dramatic change in cMIC is strongly associated with the biofilm-producing phenotype. Similarly, biofilm-producing *E. clocace*, exclusively found in day 56 wound exudates (Figure 4.1B), have become insensitive to amoxicillin, carbenicillin, and gentamicin with a cMIC well above the 100μg/mL concentration (Table 4.1). This cMIC was similar to the biofilm positive *S. epidermidis* C2, a bacterium isolated from a mouse chronic wound (31). The cMICs of biofilm-negative *Staphylococcus hominis* SP2 (147) was determined to be 2μg/mL, 6μg/mL, and 2μg/mL for amoxicillin, carbenicillin, and gentamicin, respectively (Table 4.1).

Biofilm disrupting effect of norspermidine. It has been reported that norspermidine disrupts *S. aureus* and *E. coli* biofilm production *in vitro* (45). To test whether

norspermidine can disrupt biofilms produced by bacteria that colonize *db/db* chronic wounds, we treated both day 26 and day 56 exudates and individually isolated species from those exudates with increasing concentrations of norspermidine and quantified the amount of adherent biofilms as described in the Materials and Methods. In testing, we noticed that norspermidine treatment resulted in a decrease of adherent biofilms from *db/db* bacterial communities and this effect is proportional to the concentration of norspermidine (Figure 4.2A). Our results indicate that at the 2mM concentration, we saw the greatest reduction in adherent biofilms with little to no effect on bacterial growth (Figure 4.3A). Beyond the 2mM concentration, we observed significant decline in culture turbidity quantified by optical density (data not shown). Further addition of norspermidine did not result in additional reduction in adherent biofilms. Therefore, 2mM of norspermidine was used to assess the disruption of adherence biofilms. At 2mM of norspermidine, we observed a 62±12% and 70±4% reduction in the adherent biofilms to the flat-bottomed tissue culture plate from day 26 and day 56 bacterial communities, respectively (Figure 4.2B). This reduction resulted in the decrease of 570nm optical density below the 0.125 level for day 56 (0.086±0.005) but not day 26 (0.16±0.03) bacterial communities (Figure 4.2A). In addition, norspermidine decreases the production of attached bacterial biofilms by 27±3% in *S. epidermidis* C2 (OD_{570nm} 0.70±0.03 to 0.51±0.06). Biofilm deposition can be restored to untreated levels by the removal of norspermidine (Figure 4.3B). Norspermidine did not affect *S. homonis* SP2 growth and biofilm producing capacity compared to untreated cultures (data not shown).

Community Minimal Inhibitory Concentrations			
	Amoxicillin (μg/mL)	Carbenicillin (μg/mL)	Gentamicin (μg/mL)
Day4	6	6	3
Day12	6	13	3
Day18	6	13	6
Day26	100	100	50
Day56	>100	>100	100
C2	>100	>100	>100
SP2	2	6	2

Table 4.1: The minimal concentration of antibiotics required to inhibit the growth of db/db wounds colonizing bacterial communities. The bacterial community Minimal Inhibitory Concentrations (cMIC) were determined for amoxicillin, carbenicillin, and gentamicin. Biofilm positive bacteria (day 26 and 56) are significantly more insensitive to the effects of antibiotics compared to biofilm negative bacteria (Day 4, 12, and 18). The biofilm negative and positive bacterial controls are *S. hominis* SP2 and *S. epidermidis* C2, respectively. The cMIC are reported as a range determined by three independent experiments.

Bacterial Prevalence (% Biomass)				
	Day 4	Day 18	Day 26	Day 56
S. epidermidis	25%	22%	2%	ND
Enterococcus sp.	ND	71%	59%	ND
Neisseria sp.	50%	ND	ND	ND
Pseudomonas sp.	13%	2%	6%	ND
E. cloacae	13%	5%	33%	100%
Total CFU/mL	$5.2x10^6$	$6.7x10^7$	$7.9x10^7$	$3.5x10^7$

Table 4.2: Identification of bacterial communities colonizing db/db wounds. Profile of the culturable bacterial species that colonized the *db/db* wounds show that the community is initially polymicrobic and shifted toward colonization by biofilm producing *E. cloacae* at the chronic stage. The bacteria responsible for infections are presumptively *Pseudomonas sp.*, *E. cloacae*, coagulase-negative *Staphylococcus*, and *Enterococcus sp.* ND = not detected.

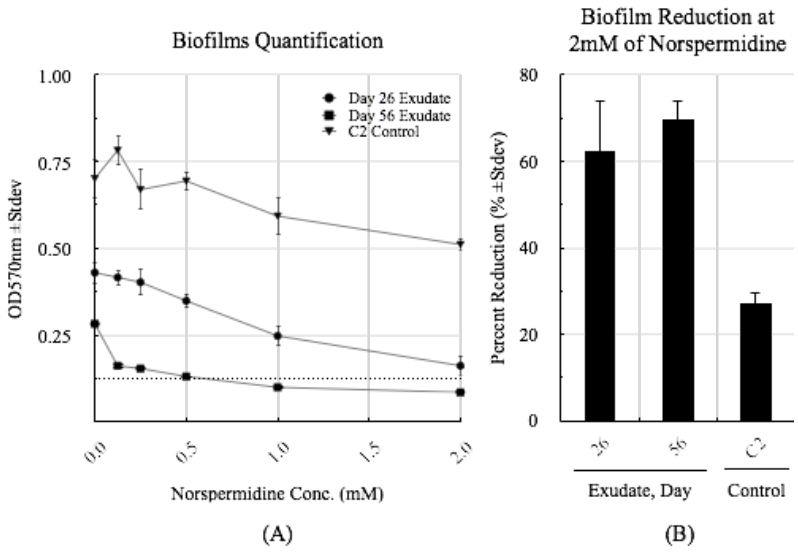

Figure 4.2: Norspermidine reduces the amount of adherent biofilms from bacterial communities from day 26 and 56 exudates. The biofilm-disassembling effect of norspermidine was measured by Hucker's crystal violet staining (left panel). The reduction of adherent submerged biofilm formation was evaluated after norspermidine treatment for 12 hours (right panel). The results are reported as the average of three independent experiments done in triplicate and the error bars indicate standard deviation. Dotted line indicates biofilm positive (above) or biofilm negative (below) community.

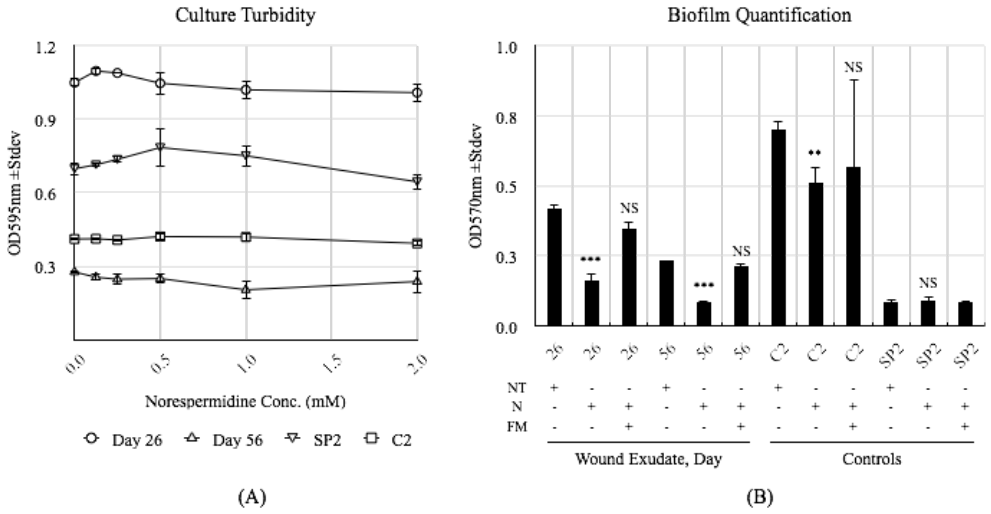

Figure 4.3: Norspermidine, at 2mM, does not affect bacterial growth and norspermidine's effect on adherent biofilms and when the biofilms are regrown in norspermidine-free media. (A) The effect of norspermidine on cell growth was quantified by calculating the change in OD_{595nm} after a 16hr incubation period. At or below 2mM, norspermidine did not affect bacterial growth. (B) After 12hr of incubation with 2mM of norspermidine (N), the production of adherent biofilms was restored to levels similarly observed prior to norspermidine treatment when grown in norspermidine free media (FM). Statistical values were obtained by comparing treated samples (N or N and FM) to its respective non-treated (NT) samples.

Antibiotic susceptibility of norspermidine treated bacterial communities. We demonstrated that biofilm positive bacterial communities are insensitive to antibiotics and norspermidine reduces adherent biofilms *in vitro*. Given our results, we hypothesized that norspermidine would positively influence the bactericidal effect of antibiotics *in vitro*. Thus, we tested whether the use of norspermidine would result in a decrease in cell survivability after exposure to gentamicin. We seeded day 26 and day 56 biofilm-positive bacterial communities onto flat-bottomed tissue culture plates, some with and without 2mM of norspermidine, for 12hr. Viable cell counts were assessed after an additional 2.5hr of exposure to gentamicin at 100μg/mL. We demonstrated that gentamicin alone was able to reduce the concentration of bacteria (measured by colony forming unit count) from day 26 and day 56; however, when used in combination with norspermidine this effect was more significantly observed (Figure 4.4). Colony-forming unit count (CFU/mL) for day 26 exudate was determined to be $7.9\pm1.2x10^7$ CFU/mL for untreated (neither gentamicin nor norspermidine) and $5.5\pm1.4x10^7$ CFU/mL for gentamicin without norspermidine samples. In the presence of norspermidine and gentamicin, we observed a 47.4% decrease in cell viability ($4.2\pm1.2x10^7$ CFU/mL) compared to the 30.9% change for gentamicin alone. Similarly, norspermidine also positively influenced the bactericidal effect of gentamicin on day 56 communities.Viable cell counts were determined to be $4.2\pm0.8x10^7$ CFU/mL for untreated, $3.5\pm0.8x10^7$ CFU/mL for gentamicin challenged, and $2.5\pm0.3x10^7$ CFU/mL for norspermidine + gentamicin treated cultures. This translated into a 60.3% decrease in cell viability compared to untreated samples and significantly enhanced the bactericidal effect of gentamicin on day 56 bacterial

communities. The norspermidine and gentamicin combination resulted in a 32.5% reduction *S. epidermidis* C2 burden compared to 23.4% reduction when gentamicin was used by itself. Furthermore, gentamicin dramatically affects *S. hominis* SP2 survival and the addition of norspermidine has little additional effect. Given these observations, we concluded that norspermidine enhances the effects of gentamicin and further decreases bacterial survivability in biofilm positive communities.

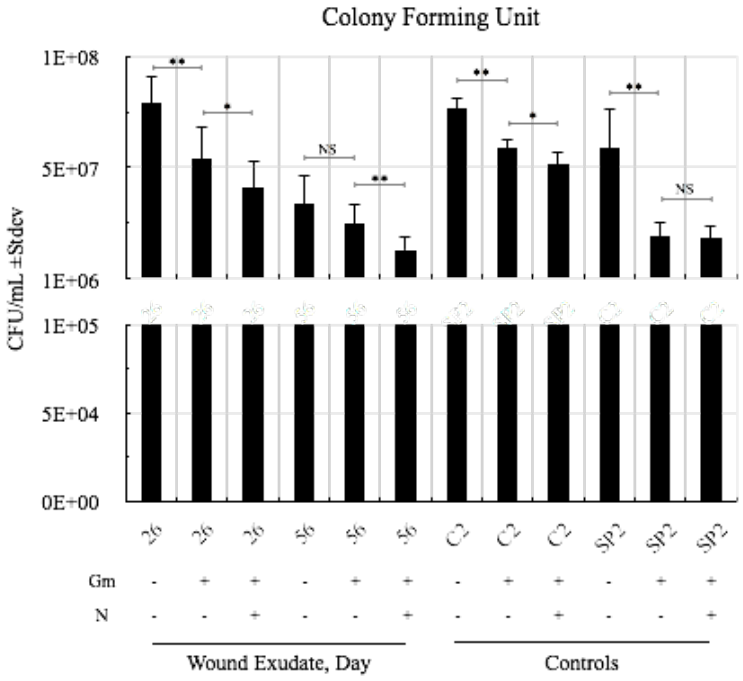

Figure 4.4: Bactericidal effect of gentamicin is increased with norspermidine. Bacterial survival in biofilms is measured by quantifying colony-forming units after 2.5hr of exposure to gentamicin. Viable cell counts show that bacteria in biofilm positive communities are more susceptible to gentamicin killing when treated with norspermidine. Norspermidine has little additional effect on the survival of non-biofilm control *S. hominis* SP2. Gm: gentamicin, and N: norspermidine.

Discussion

This study provides evidence showing that biofilms produced by the bacteria that colonized our generated *db/db* chronic wounds make the bacteria more resistant to antibiotic killing. We show that norspermidine at 2mM decreases the amount of adherent biofilms produced by the bacteria that colonize our generated *db/db* chronic wounds. Furthermore, use of norspermidine increases gentamicin bactericidal activity. As far as we know, this is the first study to evaluate the effect of norspermidine on biofilm positive bacteria that colonized chronic wounds. We believe that the use of norspermdine followed by tailored antibiotic therapy could be an effective strategy in controlling biofilm-associated bacterial infection in chronic wounds.

Bacterial communities encapsulated in a biofilm matrix are less susceptible to pharmacological agents, making them extremely difficult to eliminate (117, 148). When assessing bacterial susceptibility to commonly used β-lactam (amoxicillin and carbenicillin) and aminoglycoside (gentamicin) antibiotics, it was not surprising to see that adherent biofilm positive bacterial communities that colonized our *db/db* generated chronic wounds are insensitive to antibiotic killing. This observation is in accordance with previously published findings (117, 148).

Polyamines are well known to be involved in a variety of biological processes such as: protein translation, gene regulation, stress response, cell differentiation and growth (149). Putrescine, cadaverine, spermidine, and spermine are the predominant polyamines that are found in eukaryotes and prokaryotes (150-152). Although studies are scarce, norspermidine has been detected in many bacteria, archaea, and plants (153);

however, norspermidine is not a known polyamine that is produced in humans. The finding that norspermidine can negatively affect bacterial biofilms is the first evidence to suggest that small molecules can be catalytic for the disruption of extracellular polysaccharides (EPS) (154). Kolodkin-Gal et al. hypothesized that norspermidine specifically targeted the negatively charged or polar groups of the EPS and speculated that this weakens the secondary structure of the meshwork that hold cells together and causes the release of polymers (45). Such observations were not seen with spermidine ($C_7H_{19}N_3$) or spermine ($C_{10}H_{26}N_4$), closely related polyamines to norspermidine ($C_6H_{17}N_3$).

In contrast, norspermidine is reported to promote biofilm formation by *Vibrio cholerae* (155), the causative agent of the human diarrheal disease cholera (156). Evidence indicates that norspermidine serves as an intracellular signaling molecule that mediates the attachment of *V. cholerae* to biotic surfaces and activates the signaling components involved in biofilm formation (157). However, *V. cholerae* is not often found in human chronic wounds compared to that of various *Staphylococcus* species, *P. aeruginosa*, *Enterobacteriaceae* species, *Streptococcus* species, and *Enterococcus* species (109). Given norspermidine's broad-spectrum effect, it is conceivable to consider that application of norspermidine would cause the disruption of biofilm. As expected, norspermidine did decrease the amount of adherent biofilms *in vitro* by the bacteria that colonized our generated *db/db* chronic wounds -coagulase-negative *Staphylococcus*, hemolytic *Enterococcus sp*., *Pseudomonas sp*., and *E. cloacae*. Furthermore, prior treatment with norspermidine increases the bactericidal effect of gentamicin. Our

observations suggest that norspermidine decreases the amount of adherent biofilms, perhaps by decreasing the adherence of the EPS to the abiotic surfaces, therefore, allowing greater antibiotic access. Another possible explanation could be that the "loosening" of the EPS, caused by norspermidine allows for greater diffusion of the antibiotic through the polyanionic matrix. Similar observations to the latter explanation were documented with mucoid *P. aeruginosa* biofilms (158-161).

Although much emphasis has been placed on biofilms, it must be pointed out that a number of other factors (i.e., altered metabolic behavior, parallel gene transfers, altered microenvironment, and quorum sensing) may contribute to the ability of the bacterial community to tolerate high concentration of antibiotics (162-164). Such communal cooperative characteristics may be beneficial to the survival of the bacteria under environmental or therapeutic stress. We documented that many slow growing bacterial species isolated from our *db/db* generated chronic wounds are found in biofilm positive communities and are less sensitive to antibiotic killing compared to its faster growing counterparts (unpublished data). Antibiotic insensitivity has been reported for slow growing or starved state bacteria in biofilms (165, 166).

Given our observations, norspermidine was able to decrease the amount of adherent biofilms produced by many prominent bacterial species (e.g., *Pseudomonas*, *Staphylococcus*, *Enterococcus*, and *Enterobacter*) that are known to colonize human dermal wounds and increase the bactericidal effect of gentamicin. This in itself is an encouraging observation in the potential use of norspermidine in concert with tailored antibiotic treatments to control biofilm-associated infections in dermal wounds.

CONCLUSION OF THE DISSERTATION

In this thesis, we have demonstrated that AlgX binds alginate and site-directed mutations of the amino acids located in the CBM SRPP that participate in polysaccharide binding affect AlgX affinity to alginate. In addition, we demonstrated that the alginate-binding quality of AlgX CBM is important for alginate biosynthesis and acetylation. During alginate biosynthesis, we believe that AlgX CBM acts as an intermediate shuttle that guides the nascent alginate polymer toward the acetylation machinery and eventually to AlgE. This is the first functional demonstration of AlgX CBM's role in alginate biosynthesis and acetylation.

The chronic wound models we present in this thesis demonstrated that chronic wounds can be generated in mouse models that effectively mimic chronic wounds in humans. The model wounds stay open for weeks and capture many of the characteristics associated with human chronic wounds. We also demonstrated that biofilm associated infections and redox imbalance are the causes of turning these delayed healing wounds into chronic wounds. These wounds sustain complex biofilm associated microbiota, therefore providing insight into the biology of bacterial dynamics and host interaction and the factors that promote biofilm production. In addition, we show that restoration of the redox balance by application of antioxidant agents causes biofilms to disappear from the wounds, resulting in significant improvement in wound healing.

Lastly, we demonstrated that norspermidine reduces the amount of adherent biofilms from bacterial communities that colonized our db/db chronic wounds.

Furthermore, the use of norspermidine in combination with gentamicin increases the effect of the aminoglycoside antibiotic to kill bacteria in biofilms. This demonstrated that targeting biofilms with small molecule disruptors of biofilms could potentially be an effective strategy to combat biofilm associated bacterial infection in human chronic wounds.

References

1. **Kolter R, Greenberg EP.** 2006. Microbial sciences: the superficial life of microbes. Nature **441:**300-302.

2. **Costerton JW, Stewart PS, Greenberg EP.** 1999. Bacterial biofilms: a common cause of persistent infections. Science **284:**1318-1322.

3. **Lawrence JR, Korber DR, Hoyle BD, Costerton JW, Caldwell DE.** 1991. Optical sectioning of microbial biofilms. Journal of bacteriology **173:**6558-6567.

4. **Costerton JW, Lewandowski Z, Caldwell DE, Korber DR, Lappin-Scott HM.** 1995. Microbial biofilms. Annual review of microbiology **49:**711-745.

5. **Nickel JC, Ruseska I, Wright JB, Costerton JW.** 1985. Tobramycin resistance of *Pseudomonas aeruginosa* cells growing as a biofilm on urinary catheter material. Antimicrobial agents and chemotherapy **27:**619-624.

6. **Marrie TJ, Nelligan J, Costerton JW.** 1982. A scanning and transmission electron microscopic study of an infected endocardial pacemaker lead. Circulation **66:**1339-1341.

7. **Cohen TS, Prince A.** 2012. Cystic fibrosis: a mucosal immunodeficiency syndrome. Nature medicine **18:**509-519.

8. **Bjarnsholt T, Jensen PO, Fiandaca MJ, Pedersen J, Hansen CR, Andersen CB, Pressler T, Givskov M, Hoiby N.** 2009. *Pseudomonas aeruginosa* biofilms in the respiratory tract of cystic fibrosis patients. Pediatric pulmonology **44:**547-558.

9. **Schiotz PO, Nielsen H, Hoiby N, Glikmann G, Svehag SE.** 1978. Immune complexes in the sputum of patients with cystic fibrosis suffering from chronic *Pseudomonas aeruginosa* lung infection. Acta pathologica et microbiologica Scandinavica. Section C, Immunology **86:**37-40.

10. **Pedersen SS.** 1992. Lung infection with alginate-producing, mucoid *Pseudomonas aeruginosa* in cystic fibrosis. APMIS. Supplementum **28:**1-79.

11. **Remminghorst U, Rehm BH.** 2006. Bacterial alginates: from biosynthesis to applications. Biotechnology letters **28:**1701-1712.

12. **Banerjee PC, Vanags RI, Chakrabarty AM, Maitra PK.** 1983. Alginic acid synthesis in *Pseudomonas aeruginosa* mutants defective in carbohydrate metabolism. Journal of bacteriology **155:**238-245.

13. **May TB, Shinabarger D, Boyd A, Chakrabarty AM.** 1994. Identification of amino acid residues involved in the activity of phosphomannose isomerase-guanosine 5'-diphospho-D-mannose pyrophosphorylase. A bifunctional enzyme in the alginate biosynthetic pathway of *Pseudomonas aeruginosa*. The Journal of biological chemistry **269:**4872-4877.

14. **Olvera C, Goldberg JB, Sanchez R, Soberon-Chavez G.** 1999. The *Pseudomonas aeruginosa* algC gene product participates in rhamnolipid biosynthesis. FEMS microbiology letters **179:**85-90.

15. **Oglesby LL, Jain S, Ohman DE.** 2008. Membrane topology and roles of *Pseudomonas aeruginosa* Alg8 and Alg44 in alginate polymerization. Microbiology **154:**1605-1615.

16. **Rehm BHA.** 2009. Alginate Production: Precursor Biosynthesis, Polymerization and Secretion, p. 55-67. *In* Rehm BHA (ed.), Alginates: Biology and Applications Microbiology Monographs 13. Springer-Verlag Berlin Heidelberg

17. **Pindar DF, Bucke C.** 1975. The biosynthesis of alginic acid by *Azotobacter vinelandii*. The Biochemical journal **152:**617-622.

18. **Monday SR, Schiller NL.** 1996. Alginate synthesis in *Pseudomonas aeruginosa*: the role of AlgL (alginate lyase) and AlgX. Journal of bacteriology **178:**625-632.

19. **Robles-Price A, Wong TY, Sletta H, Valla S, Schiller NL.** 2004. AlgX is a periplasmic protein required for alginate biosynthesis in *Pseudomonas aeruginosa*. Journal of bacteriology **186:**7369-7377.

20. **Franklin MJ, Chitnis CE, Gacesa P, Sonesson A, White DC, Ohman DE.** 1994. *Pseudomonas aeruginosa* AlgG is a polymer level alginate C5-mannuronan epimerase. Journal of bacteriology **176:**1821-1830.

21. **Jain S, Ohman DE.** 1998. Deletion of *algK* in mucoid *Pseudomonas aeruginosa* blocks alginate polymer formation and results in uronic acid secretion. Journal of bacteriology **180:**634-641.

22. **Riley LM, Weadge JT, Baker P, Robinson H, Codee JD, Tipton PA, Ohman DE, Howell PL.** 2013. Structural and functional characterization of *Pseudomonas aeruginosa* AlgX: role of AlgX in alginate acetylation. The Journal of biological chemistry **288:**22299-22314.

23. **Bjarnsholt T, Kirketerp-Moller K, Jensen PO, Madsen KG, Phipps R, Krogfelt K, Hoiby N, Givskov M.** 2008. Why chronic wounds will not heal: a novel hypothesis. Wound repair and regeneration : official publication of the Wound Healing Society [and] the European Tissue Repair Society **16:**2-10.

24. **Kim PJ, Steinberg JS.** 2012. Wound care: biofilm and its impact on the latest treatment modalities for ulcerations of the diabetic foot. Seminars in vascular surgery **25:**70-74.

25. **Davies DG, Chakrabarty AM, Geesey GG.** 1993. Exopolysaccharide production in biofilms: substratum activation of alginate gene expression by *Pseudomonas aeruginosa*. Applied and environmental microbiology **59:**1181-1186.

26. **Siddiqui AR, Bernstein JM.** 2010. Chronic wound infection: facts and controversies. Clinics in dermatology **28:**519-526.

27. **Schaber JA, Triffo WJ, Suh SJ, Oliver JW, Hastert MC, Griswold JA, Auer M, Hamood AN, Rumbaugh KP.** 2007. *Pseudomonas aeruginosa* forms biofilms in acute infection independent of cell-to-cell signaling. Infection and immunity **75:**3715-3721.

28. **Hendricks KJ, Burd TA, Anglen JO, Simpson AW, Christensen GD, Gainor BJ.** 2001. Synergy between *Staphylococcus aureus* and *Pseudomonas aeruginosa* in a rat model of complex orthopaedic wounds. The Journal of bone and joint surgery. American volume **83-A:**855-861.

29. **Mastropaolo MD, Evans NP, Byrnes MK, Stevens AM, Robertson JL, Melville SB.** 2005. Synergy in polymicrobial infections in a mouse model of type 2 diabetes. Infection and immunity **73:**6055-6063.

30. **Dalton T, Dowd SE, Wolcott RD, Sun Y, Watters C, Griswold JA, Rumbaugh KP.** 2011. An *in vivo* polymicrobial biofilm wound infection model to study interspecies interactions. PloS one **6:**e27317.

31. **Petreaca ML, Do D, Dhall S, McLelland D, Serafino A, Lyubovitsky J, Schiller N, Martins-Green MM.** 2012. Deletion of a tumor necrosis superfamily gene in mice leads to impaired healing that mimics chronic wounds in humans. Wound repair and regeneration : official publication of the Wound Healing Society [and] the European Tissue Repair Society **20:**353-366.

32. **Petreaca ML, Dhall S, McClelland DL, Serafino A, Do D, Lyubovitsky J, Schiller N, Martins-Green M.** 2011. Impaired healing in a genetically modified

mouse mimics venus ulcers in humans. Wound repair and regeneration : official publication of the Wound Healing Society [and] the European Tissue Repair Society **19:**A42-A42.

33. **Sen CK, Gordillo GM, Roy S, Kirsner R, Lambert L, Hunt TK, Gottrup F, Gurtner GC, Longaker MT.** 2009. Human skin wounds: a major and snowballing threat to public health and the economy. Wound repair and regeneration : official publication of the Wound Healing Society [and] the European Tissue Repair Society **17:**763-771.

34. **Wlaschek M, Scharffetter-Kochanek K.** 2005. Oxidative stress in chronic venous leg ulcers. Wound repair and regeneration : official publication of the Wound Healing Society [and] the European Tissue Repair Society **13:**452-461.

35. **James TJ, Hughes MA, Cherry GW, Taylor RP.** 2003. Evidence of oxidative stress in chronic venous ulcers. Wound repair and regeneration : official publication of the Wound Healing Society [and] the European Tissue Repair Society **11:**172-176.

36. **James GA, Swogger E, Wolcott R, Pulcini E, Secor P, Sestrich J, Costerton JW, Stewart PS.** 2008. Biofilms in chronic wounds. Wound repair and regeneration : official publication of the Wound Healing Society [and] the European Tissue Repair Society **16:**37-44.

37. **Roy S, Khanna S, Nallu K, Hunt TK, Sen CK.** 2006. Dermal wound healing is subject to redox control. Molecular therapy : the journal of the American Society of Gene Therapy **13:**211-220.

38. **D'Autreaux B, Toledano MB.** 2007. ROS as signalling molecules: mechanisms that generate specificity in ROS homeostasis. Nature reviews. Molecular cell biology **8:**813-824.

39. **Sen CK, Roy S.** 2008. Redox signals in wound healing. Biochimica et biophysica acta **1780:**1348-1361.

40. **Yeoh-Ellerton S, Stacey MC.** 2003. Iron and 8-isoprostane levels in acute and chronic wounds. The Journal of investigative dermatology **121:**918-925.

41. **Yang Q, Phillips PL, Sampson EM, Progulske-Fox A, Jin S, Antonelli P, Schultz GS.** 2013. Development of a novel ex vivo porcine skin explant model for the assessment of mature bacterial biofilms. Wound repair and regeneration : official publication of the Wound Healing Society [and] the European Tissue Repair Society **21:**704-714.

42. **Gjodsbol K, Christensen JJ, Karlsmark T, Jorgensen B, Klein BM, Krogfelt KA.** 2006. Multiple bacterial species reside in chronic wounds: a longitudinal study. International wound journal **3:**225-231.

43. **Shadnia S, Dasgar M, Taghikhani S, Mohammadirad A, Khorasani R, Abdollahi M.** 2007. Protective Effects of alpha-Tocopherol and N-Acetyl-Cysteine on Diazinon-Induced Oxidative Stress and Acetylcholinesterase Inhibition in Rats. Toxicology mechanisms and methods **17:**109-115.

44. **Karatan E, Watnick P.** 2009. Signals, regulatory networks, and materials that build and break bacterial biofilms. Microbiology and molecular biology reviews : MMBR **73:**310-347.

45. **Kolodkin-Gal I, Cao S, Chai L, Bottcher T, Kolter R, Clardy J, Losick R.** 2012. A self-produced trigger for biofilm disassembly that targets exopolysaccharide. Cell **149:**684-692.

46. **Kolodkin-Gal I, Romero D, Cao S, Clardy J, Kolter R, Losick R.** 2010. D-amino acids trigger biofilm disassembly. Science **328:**627-629.

47. **Kerem B, Rommens JM, Buchanan JA, Markiewicz D, Cox TK, Chakravarti A, Buchwald M, Tsui LC.** 1989. Identification of the cystic fibrosis gene: genetic analysis. Science **245:**1073-1080.

48. **Riordan JR, Rommens JM, Kerem B, Alon N, Rozmahel R, Grzelczak Z, Zielenski J, Lok S, Plavsic N, Chou JL, et al.** 1989. Identification of the cystic fibrosis gene: cloning and characterization of complementary DNA. Science **245:**1066-1073.

49. **Rommens JM, Iannuzzi MC, Kerem B, Drumm ML, Melmer G, Dean M, Rozmahel R, Cole JL, Kennedy D, Hidaka N, et al.** 1989. Identification of the cystic fibrosis gene: chromosome walking and jumping. Science **245:**1059-1065.

50. **Cheng SH, Gregory RJ, Marshall J, Paul S, Souza DW, White GA, O'Riordan CR, Smith AE.** 1990. Defective intracellular transport and processing of CFTR is the molecular basis of most cystic fibrosis. Cell **63:**827-834.

51. **Pier GB.** 1985. Pulmonary disease associated with *Pseudomonas aeruginosa* in cystic fibrosis: current status of the host-bacterium interaction. The Journal of infectious diseases **151:**575-580.

52. **Gibson RL, Burns JL, Ramsey BW.** 2003. Pathophysiology and management of pulmonary infections in cystic fibrosis. American journal of respiratory and critical care medicine **168:**918-951.

53. **Rehm BH, Valla S.** 1997. Bacterial alginates: biosynthesis and applications. Applied microbiology and biotechnology **48:**281-288.

54. **Krieg DP, Helmke RJ, German VF, Mangos JA.** 1988. Resistance of mucoid *Pseudomonas aeruginosa* to nonopsonic phagocytosis by alveolar macrophages in vitro. Infection and immunity **56:**3173-3179.

55. **Simpson JA, Smith SE, Dean RT.** 1988. Alginate inhibition of the uptake of *Pseudomonas aeruginosa* by macrophages. Journal of general microbiology **134:**29-36.

56. **Simpson JA, Smith SE, Dean RT.** 1989. Scavenging by alginate of free radicals released by macrophages. Free radical biology & medicine **6:**347-353.

57. **DeVries CA, Ohman DE.** 1994. Mucoid-to-nonmucoid conversion in alginate-producing *Pseudomonas aeruginosa* often results from spontaneous mutations in *algT*, encoding a putative alternate sigma factor, and shows evidence for autoregulation. Journal of bacteriology **176:**6677-6687.

58. **Martin DW, Holloway BW, Deretic V.** 1993. Characterization of a locus determining the mucoid status of *Pseudomonas aeruginosa*: AlgU shows sequence similarities with a *Bacillus* sigma factor. Journal of bacteriology **175:**1153-1164.

59. **Schurr MJ, Yu H, Martinez-Salazar JM, Boucher JC, Deretic V.** 1996. Control of AlgU, a member of the sigma E-like family of stress sigma factors, by the negative regulators MucA and MucB and *Pseudomonas aeruginosa* conversion to mucoidy in cystic fibrosis. Journal of bacteriology **178:**4997-5004.

60. **Xie ZD, Hershberger CD, Shankar S, Ye RW, Chakrabarty AM.** 1996. Sigma factor-anti-sigma factor interaction in alginate synthesis: inhibition of AlgT by MucA. Journal of bacteriology **178:**4990-4996.

61. **Ohman DE.** 2009. Alginate gene regulation, p. 117-133. *In* Rehm BHA (ed.), Alginates: Biology and Applications. Springer Berlin Heidelberg.

62. **Martin DW, Schurr MJ, Mudd MH, Govan JR, Holloway BW, Deretic V.** 1993. Mechanism of conversion to mucoidy in *Pseudomonas aeruginosa* infecting cystic fibrosis patients. Proceedings of the National Academy of Sciences of the United States of America **90:**8377-8381.

63. **Hershberger CD, Ye RW, Parsek MR, Xie ZD, Chakrabarty AM.** 1995. The *algT* (*algU*) gene of *Pseudomonas aeruginosa*, a key regulator involved in alginate biosynthesis, encodes an alternative sigma factor (sigma E). Proceedings

of the National Academy of Sciences of the United States of America **92:**7941-7945.

64. **Shankar S, Ye RW, Schlictman D, Chakrabarty AM.** 1995. Exopolysaccharide alginate synthesis in *Pseudomonas aeruginosa*: enzymology and regulation of gene expression. Advances in enzymology and related areas of molecular biology **70:**221-255.

65. **Mathee K, McPherson CJ, Ohman DE.** 1997. Posttranslational control of the *algT* (*algU*)-encoded sigma22 for expression of the alginate regulon in *Pseudomonas aeruginosa* and localization of its antagonist proteins MucA and MucB (AlgN). Journal of bacteriology **179:**3711-3720.

66. **Gacesa P.** 1998. Bacterial alginate biosynthesis--recent progress and future prospects. Microbiology **144 (Pt 5):**1133-1143.

67. **Goldberg JB, Hatano K, Pier GB.** 1993. Synthesis of lipopolysaccharide O side chains by *Pseudomonas aeruginosa* PAO1 requires the enzyme phosphomannomutase. Journal of bacteriology **175:**1605-1611.

68. **Tatnell PJ, Russell NJ, Gacesa P.** 1993. A metabolic study of the activity of GDP-mannose dehydrogenase and concentrations of activated intermediates of alginate biosynthesis in *Pseudomonas aeruginosa*. Journal of general microbiology **139:**119-127.

69. **Tatnell PJ, Russell NJ, Gacesa P.** 1994. GDP-mannose dehydrogenase is the key regulatory enzyme in alginate biosynthesis in *Pseudomonas aeruginosa*: evidence from metabolite studies. Microbiology **140 (Pt 7):**1745-1754.

70. **Ye RW, Zielinski NA, Chakrabarty AM.** 1994. Purification and characterization of phosphomannomutase/phosphoglucomutase from *Pseudomonas aeruginosa* involved in biosynthesis of both alginate and lipopolysaccharide. Journal of bacteriology **176:**4851-4857.

71. **Grabert E, Wingender J, Winkler UK.** 1990. An outer membrane protein characteristic of mucoid strains of *Pseudomonas aeruginosa*. FEMS microbiology letters **56:**83-87.

72. **Chu L, May TB, Chakrabarty AM, Misra TK.** 1991. Nucleotide sequence and expression of the *algE* gene involved in alginate biosynthesis by *Pseudomonas aeruginosa*. Gene **107:**1-10.

73. **Saxena IM, Brown RM, Jr.** 1995. Identification of a second cellulose synthase gene (*acsAII*) in *Acetobacter xylinum*. Journal of bacteriology **177:**5276-5283.

74. **Saxena IM, Brown RM, Jr., Dandekar T.** 2001. Structure--function characterization of cellulose synthase: relationship to other glycosyltransferases. Phytochemistry **57:**1135-1148.

75. **Chitnis CE, Ohman DE.** 1990. Cloning of *Pseudomonas aeruginosa algG*, which controls alginate structure. Journal of bacteriology **172:**2894-2900.

76. **Schiller NL, Monday SR, Boyd CM, Keen NT, Ohman DE.** 1993. Characterization of the *Pseudomonas aeruginosa* alginate lyase gene (*algL*): cloning, sequencing, and expression in *Escherichia coli*. Journal of bacteriology **175:**4780-4789.

77. **Franklin MJ, Ohman DE.** 1996. Identification of *algI* and *algJ* in the *Pseudomonas aeruginosa* alginate biosynthetic gene cluster which are required for alginate O acetylation. Journal of bacteriology **178:**2186-2195.

78. **Gimmestad M, Sletta H, Ertesvag H, Bakkevig K, Jain S, Suh SJ, Skjak-Braek G, Ellingsen TE, Ohman DE, Valla S.** 2003. The *Pseudomonas fluorescens* AlgG protein, but not its mannuronan C-5-epimerase activity, is needed for alginate polymer formation. Journal of bacteriology **185:**3515-3523.

79. **Franklin MJ, Douthit SA, McClure MA.** 2004. Evidence that the *algI/algJ* gene cassette, required for O acetylation of *Pseudomonas aeruginosa* alginate, evolved by lateral gene transfer. Journal of bacteriology **186:**4759-4773.

80. **Jain S, Ohman DE.** 2005. Role of an alginate lyase for alginate transport in mucoid *Pseudomonas aeruginosa*. Infection and immunity **73:**6429-6436.

81. **Albrecht MT, Schiller NL.** 2005. Alginate lyase (AlgL) activity is required for alginate biosynthesis in *Pseudomonas aeruginosa*. Journal of bacteriology **187:**3869-3872.

82. **Aarons SJ, Sutherland IW, Chakrabarty AM, Gallagher MP.** 1997. A novel gene, *algK*, from the alginate biosynthesis cluster of *Pseudomonas aeruginosa*. Microbiology **143 (Pt 2):**641-652.

83. **Keiski CL, Harwich M, Jain S, Neculai AM, Yip P, Robinson H, Whitney JC, Riley L, Burrows LL, Ohman DE, Howell PL.** 2010. AlgK is a TPR-containing protein and the periplasmic component of a novel exopolysaccharide secretin. Structure **18:**265-273.

84. **Hay ID, Schmidt O, Filitcheva J, Rehm BH.** 2012. Identification of a periplasmic AlgK-AlgX-MucD multiprotein complex in *Pseudomonas*

aeruginosa involved in biosynthesis and regulation of alginate. Applied microbiology and biotechnology **93:**215-227.

85. **Weadge JT, Yip PP, Robinson H, Arnett K, Tipton PA, Howell PL.** 2010. Expression, purification, crystallization and preliminary X-ray analysis of *Pseudomonas aeruginosa* AlgX. Acta crystallographica. Section F, Structural biology and crystallization communications **66:**588-591.

86. **Stover CK, Pham XQ, Erwin AL, Mizoguchi SD, Warrener P, Hickey MJ, Brinkman FS, Hufnagle WO, Kowalik DJ, Lagrou M, Garber RL, Goltry L, Tolentino E, Westbrock-Wadman S, Yuan Y, Brody LL, Coulter SN, Folger KR, Kas A, Larbig K, Lim R, Smith K, Spencer D, Wong GK, Wu Z, Paulsen IT, Reizer J, Saier MH, Hancock RE, Lory S, Olson MV.** 2000. Complete genome sequence of *Pseudomonas aeruginosa* PAO1, an opportunistic pathogen. Nature **406:**959-964.

87. **Schweizer HP.** 1991. *Escherichia-Pseudomonas* shuttle vectors derived from pUC18/19. Gene **97:**109-121.

88. **Diver JM, Bryan LE, Sokol PA.** 1990. Transformation of *Pseudomonas aeruginosa* by electroporation. Analytical biochemistry **189:**75-79.

89. **Phadnis SH, Berg DE.** 1987. Identification of base pairs in the outside end of insertion sequence IS50 that are needed for IS50 and Tn5 transposition. Proceedings of the National Academy of Sciences of the United States of America **84:**9118-9122.

90. **Knutson CA, Jeanes A.** 1968. A new modification of the carbazole analysis: application to heteropolysaccharides. Analytical biochemistry **24:**470-481.

91. **Pedersen SS, Espersen F, Hoiby N, Shand GH.** 1989. Purification, characterization, and immunological cross-reactivity of alginates produced by mucoid *Pseudomonas aeruginosa* from patients with cystic fibrosis. Journal of clinical microbiology **27:**691-699.

92. **Hestrin S.** 1949. The reaction of acetylcholine and other carboxylic acid derivatives with hydroxylamine, and its analytical application. The Journal of biological chemistry **180:**249-261.

93. **Larkin MA, Blackshields G, Brown NP, Chenna R, McGettigan PA, McWilliam H, Valentin F, Wallace IM, Wilm A, Lopez R, Thompson JD, Gibson TJ, Higgins DG.** 2007. Clustal W and Clustal X version 2.0. Bioinformatics **23:**2947-2948.

94. **Eswar N, Webb B, Marti-Renom MA, Madhusudhan MS, Eramian D, Shen MY, Pieper U, Sali A.** 2007. Comparative protein structure modeling using MODELLER. Current protocols in protein science / editorial board, John E. Coligan ... [et al.] **Chapter 2:**Unit 2 9.

95. **Jamroz M, Kolinski A.** 2010. Modeling of loops in proteins: a multi-method approach. BMC structural biology **10:**5.

96. **Rozeboom HJ, Bjerkan TM, Kalk KH, Ertesvag H, Holtan S, Aachmann FL, Valla S, Dijkstra BW.** 2008. Structural and mutational characterization of the catalytic A-module of the mannuronan C-5-epimerase AlgE4 from *Azotobacter vinelandii*. The Journal of biological chemistry **283:**23819-23828.

97. **Yoon HJ, Hashimoto W, Miyake O, Murata K, Mikami B.** 2001. Crystal structure of alginate lyase A1-III complexed with trisaccharide product at 2.0 A resolution. Journal of molecular biology **307:**9-16.

98. **Momma K, Mishima Y, Hashimoto W, Mikami B, Murata K.** 2005. Direct evidence for *Sphingomonas sp.* A1 periplasmic proteins as macromolecule-binding proteins associated with the ABC transporter: molecular insights into alginate transport in the periplasm. Biochemistry **44:**5053-5064.

99. **Trott O, Olson AJ.** 2010. AutoDock Vina: improving the speed and accuracy of docking with a new scoring function, efficient optimization, and multithreading. Journal of computational chemistry **31:**455-461.

100. **Morris GM, Huey R, Lindstrom W, Sanner MF, Belew RK, Goodsell DS, Olson AJ.** 2009. AutoDock4 and AutoDockTools4: Automated docking with selective receptor flexibility. Journal of computational chemistry **30:**2785-2791.

101. **Grant BJ, Rodrigues AP, ElSawy KM, McCammon JA, Caves LS.** 2006. Bio3d: an R package for the comparative analysis of protein structures. Bioinformatics **22:**2695-2696.

102. **Pettersen EF, Goddard TD, Huang CC, Couch GS, Greenblatt DM, Meng EC, Ferrin TE.** 2004. UCSF Chimera--a visualization system for exploratory research and analysis. Journal of computational chemistry **25:**1605-1612.

103. **Yamasaki M, Moriwaki S, Miyake O, Hashimoto W, Murata K, Mikami B.** 2004. Structure and function of a hypothetical *Pseudomonas aeruginosa* protein PA1167 classified into family PL-7: a novel alginate lyase with a beta-sandwich fold. The Journal of biological chemistry **279:**31863-31872.

104. **Boyd A, Ghosh M, May TB, Shinabarger D, Keogh R, Chakrabarty AM.** 1993. Sequence of the *algL* gene of *Pseudomonas aeruginosa* and purification of its alginate lyase product. Gene **131:**1-8.

105. **Tomme P, Warren RA, Gilkes NR.** 1995. Cellulose hydrolysis by bacteria and fungi. Advances in microbial physiology **37:**1-81.

106. **Beguin P, Aubert JP.** 1994. The biological degradation of cellulose. FEMS microbiology reviews **13:**25-58.

107. **Lazarus GS, Cooper DM, Knighton DR, Percoraro RE, Rodeheaver G, Robson MC.** 1994. Definitions and guidelines for assessment of wounds and evaluation of healing. Wound repair and regeneration : official publication of the Wound Healing Society [and] the European Tissue Repair Society **2:**165-170.

108. **Wong VW, Gurtner GC.** 2012. Tissue engineering for the management of chronic wounds: current concepts and future perspectives. Experimental dermatology **21:**729-734.

109. **Howell-Jones RS, Wilson MJ, Hill KE, Howard AJ, Price PE, Thomas DW.** 2005. A review of the microbiology, antibiotic usage and resistance in chronic skin wounds. The Journal of antimicrobial chemotherapy **55:**143-149.

110. **Margoliash E, Novogrodsky A, Schejter A.** 1960. Irreversible reaction of 3-amino-1:2:4-triazole and related inhibitors with the protein of catalase. The Biochemical journal **74:**339-348.

111. **Chaudiere J, Wilhelmsen EC, Tappel AL.** 1984. Mechanism of selenium-glutathione peroxidase and its inhibition by mercaptocarboxylic acids and other mercaptans. The Journal of biological chemistry **259:**1043-1050.

112. **Christensen GD, Simpson WA, Younger JJ, Baddour LM, Barrett FF, Melton DM, Beachey EH.** 1985. Adherence of coagulase-negative staphylococci to plastic tissue culture plates: a quantitative model for the adherence of staphylococci to medical devices. Journal of clinical microbiology **22:**996-1006.

113. **Handy DE, Lubos E, Yang Y, Galbraith JD, Kelly N, Zhang YY, Leopold JA, Loscalzo J.** 2009. Glutathione peroxidase-1 regulates mitochondrial function to modulate redox-dependent cellular responses. The Journal of biological chemistry **284:**11913-11921.

114. **Antunes F, Han D, Cadenas E.** 2002. Relative contributions of heart mitochondria glutathione peroxidase and catalase to H(2)O(2) detoxification in in vivo conditions. Free radical biology & medicine **33:**1260-1267.

115. **O'Toole GA, Kolter R.** 1998. Initiation of biofilm formation in *Pseudomonas fluorescens* WCS365 proceeds via multiple, convergent signalling pathways: a genetic analysis. Molecular microbiology **28:**449-461.

116. **Stepanovic S, Vukovic D, Dakic I, Savic B, Svabic-Vlahovic M.** 2000. A modified microtiter-plate test for quantification of staphylococcal biofilm formation. Journal of microbiological methods **40:**175-179.

117. **Percival SL, Hill KE, Malic S, Thomas DW, Williams DW.** 2011. Antimicrobial tolerance and the significance of persister cells in recalcitrant chronic wound biofilms. Wound repair and regeneration : official publication of the Wound Healing Society [and] the European Tissue Repair Society **19:**1-9.

118. **Parsek MR, Singh PK.** 2003. Bacterial biofilms: an emerging link to disease pathogenesis. Annual review of microbiology **57:**677-701.

119. **Cho I, Blaser MJ.** 2012. The human microbiome: at the interface of health and disease. Nature reviews. Genetics **13:**260-270.

120. **Kerksick C, Willoughby D.** 2005. The antioxidant role of glutathione and N-acetyl-cysteine supplements and exercise-induced oxidative stress. Journal of the International Society of Sports Nutrition **2:**38-44.

121. **Brigelius-Flohe R, Traber MG.** 1999. Vitamin E: function and metabolism. FASEB journal : official publication of the Federation of American Societies for Experimental Biology **13:**1145-1155.

122. **Herrera E, Barbas C.** 2001. Vitamin E: action, metabolism and perspectives. Journal of physiology and biochemistry **57:**43-56.

123. **Packer L, Weber SU, Rimbach G.** 2001. Molecular aspects of alpha-tocotrienol antioxidant action and cell signalling. The Journal of nutrition **131:**369S-373S.

124. **Zhao G, Usui ML, Underwood RA, Singh PK, James GA, Stewart PS, Fleckman P, Olerud JE.** 2012. Time course study of delayed wound healing in a biofilm-challenged diabetic mouse model. Wound repair and regeneration : official publication of the Wound Healing Society [and] the European Tissue Repair Society **20:**342-352.

125. **Scales BS, Huffnagle GB.** 2013. The microbiome in wound repair and tissue fibrosis. The Journal of pathology **229:**323-331.

126. **Sommers HM.** 1985. The Biologic and Clinical Basis of Infectious Diseases, P. Youmans, P. Y. Paterson, and H. M. Sommers ed. Saunders, Philadelphia, Pa.

127. **Grice EA, Segre JA.** 2011. The skin microbiome. Nature reviews. Microbiology **9:**244-253.

128. **Dalben M, Varkulja G, Basso M, Krebs VL, Gibelli MA, van der Heijden I, Rossi F, Duboc G, Levin AS, Costa SF.** 2008. Investigation of an outbreak of *Enterobacter cloacae* in a neonatal unit and review of the literature. The Journal of hospital infection **70:**7-14.

129. **Madsen SM, Westh H, Danielsen L, Rosdahl VT.** 1996. Bacterial colonization and healing of venous leg ulcers. APMIS : acta pathologica, microbiologica, et immunologica Scandinavica **104:**895-899.

130. **Gerding DN.** 1995. Foot infections in diabetic patients: the role of anaerobes. Clinical infectious diseases : an official publication of the Infectious Diseases Society of America **20 Suppl 2:**S283-288.

131. **Sapico FL, Witte JL, Canawati HN, Montgomerie JZ, Bessman AN.** 1984. The infected foot of the diabetic patient: quantitative microbiology and analysis of clinical features. Reviews of infectious diseases **6 Suppl 1:**S171-176.

132. **Sharp CS, Bessman AN, Wagner FW, Jr., Garland D.** 1978. Microbiology of deep tissue in diabetic gangrene. Diabetes care **1:**289-292.

133. **Hansson C, Hoborn J, Moller A, Swanbeck G.** 1995. The microbial flora in venous leg ulcers without clinical signs of infection. Repeated culture using a validated standardised microbiological technique. Acta dermato-venereologica **75:**24-30.

134. **Roth RR, James WD.** 1988. Microbial ecology of the skin. Annual review of microbiology **42:**441-464.

135. **Brook I, Frazier EH.** 1998. Aerobic and anaerobic microbiology of chronic venous ulcers. International journal of dermatology **37:**426-428.

136. **Sebeny PJ, Riddle MS, Petersen K.** 2008. *Acinetobacter baumannii* skin and soft-tissue infection associated with war trauma. Clinical infectious diseases : an official publication of the Infectious Diseases Society of America **47:**444-449.

137. **Dowd SE, Sun Y, Secor PR, Rhoads DD, Wolcott BM, James GA, Wolcott RD.** 2008. Survey of bacterial diversity in chronic wounds using pyrosequencing, DGGE, and full ribosome shotgun sequencing. BMC microbiology **8:**43.

138. **Be NA, Allen JE, Brown TS, Gardner SN, McLoughlin KS, Forsberg JA, Kirkup BC, Chromy BA, Luciw PA, Elster EA, Jaing CJ.** 2014. Microbial Profiling of Combat Wound Infection through Detection Microarray and Next-Generation Sequencing. Journal of clinical microbiology **52:**2583-2594.

139. **Hall-Stoodley L, Costerton JW, Stoodley P.** 2004. Bacterial biofilms: from the natural environment to infectious diseases. Nature reviews. Microbiology **2:**95-108.

140. **Percival SL, Hill KE, Williams DW, Hooper SJ, Thomas DW, Costerton JW.** 2012. A review of the scientific evidence for biofilms in wounds. Wound repair and regeneration : official publication of the Wound Healing Society [and] the European Tissue Repair Society **20:**647-657.

141. **Woods E, Davis P, Barnett J, Percival SL.** 2010. Wound healing, immunology and biofilms. CRC Press, London, UK.

142. **Shigeta M, Tanaka G, Komatsuzawa H, Sugai M, Suginaka H, Usui T.** 1997. Permeation of antimicrobial agents through *Pseudomonas aeruginosa* biofilms: a simple method. Chemotherapy **43:**340-345.

143. **Williams P.** 1994. Host immune defences and biofilms. BioLine, Cardiff, UK.

144. **Johnson GM, Lee DA, Regelmann WE, Gray ED, Peters G, Quie PG.** 1986. Interference with granulocyte function by *Staphylococcus epidermidis* slime. Infection and immunity **54:**13-20.

145. **Hochbaum AI, Kolodkin-Gal I, Foulston L, Kolter R, Aizenberg J, Losick R.** 2011. Inhibitory effects of D-amino acids on *Staphylococcus aureus* biofilm development. Journal of bacteriology **193:**5616-5622.

146. **Sonnenwirth AC.** 1980. Stains and staining procedures, p. 1380. *In* Sonnenwirth, Jarett L (ed.), Gradwohl's clinical laboratory methods and diagnosis, vol. 8. The C.V. Mosby Co., St. Louis.

147. **Qu Y, Daley AJ, Istivan TS, Garland SM, Deighton MA.** 2010. Antibiotic susceptibility of coagulase-negative staphylococci isolated from very low birth weight babies: comprehensive comparisons of bacteria at different stages of biofilm formation. Annals of clinical microbiology and antimicrobials **9:**16.

148. **Hoyle BD, Costerton JW.** 1991. Bacterial resistance to antibiotics: the role of biofilms. Progress in drug research. Fortschritte der Arzneimittelforschung. Progres des recherches pharmaceutiques **37:**91-105.

149. **Igarashi K, Kashiwagi K.** 2010. Modulation of cellular function by polyamines. The international journal of biochemistry & cell biology **42:**39-51.

150. **Rodriguez-Garay B, Phillips GC, Kuehn GD.** 1989. Detection of Norspermidine and Norspermine in Medicago sativa L. (Alfalfa). Plant physiology **89:**525-529.

151. **Yamamoto S, Shinoda S, Makita M.** 1979. Occurrence of norspermidine in some species of genera *Vibrio* and *Beneckea*. Biochemical and biophysical research communications **87:**1102-1108.

152. **Hamana K, Matsuzaki S.** 1982. Widespread occurrence of norspermidine and norspermine in eukaryotic algae. Journal of biochemistry **91:**1321-1328.

153. **Di Martino ML, Campilongo R, Casalino M, Micheli G, Colonna B, Prosseda G.** 2013. Polyamines: emerging players in bacteria-host interactions. International journal of medical microbiology : IJMM **303:**484-491.

154. **Oppenheimer-Shaanan Y, Steinberg N, Kolodkin-Gal I.** 2013. Small molecules are natural triggers for the disassembly of biofilms. Trends in microbiology **21:**594-601.

155. **Lee J, Sperandio V, Frantz DE, Longgood J, Camilli A, Phillips MA, Michael AJ.** 2009. An alternative polyamine biosynthetic pathway is widespread in bacteria and essential for biofilm formation in *Vibrio cholerae*. The Journal of biological chemistry **284:**9899-9907.

156. **Faruque SM, Albert MJ, Mekalanos JJ.** 1998. Epidemiology, genetics, and ecology of toxigenic *Vibrio cholerae*. Microbiology and molecular biology reviews : MMBR **62:**1301-1314.

157. **Karatan E, Duncan TR, Watnick PI.** 2005. NspS, a predicted polyamine sensor, mediates activation of *Vibrio cholerae* biofilm formation by norspermidine. Journal of bacteriology **187:**7434-7443.

158. **Hatch RA, Schiller NL.** 1998. Alginate lyase promotes diffusion of aminoglycosides through the extracellular polysaccharide of mucoid *Pseudomonas aeruginosa*. Antimicrobial agents and chemotherapy **42:**974-977.

159. **Alkawash MA, Soothill JS, Schiller NL.** 2006. Alginate lyase enhances antibiotic killing of mucoid *Pseudomonas aeruginosa* in biofilms. APMIS : acta pathologica, microbiologica, et immunologica Scandinavica **114:**131-138.

160. **Allison DG, Matthews MJ.** 1992. Effect of polysaccharide interactions on antibiotic susceptibility of *Pseudomonas aeruginosa*. The Journal of applied bacteriology **73:**484-488.

161. **Nichols WW, Dorrington SM, Slack MP, Walmsley HL.** 1988. Inhibition of tobramycin diffusion by binding to alginate. Antimicrobial agents and chemotherapy **32:**518-523.

162. **Percival SL, Bowler PG.** 2004. Biofilms and their potential role in wound healing. Wounds **16:**234-240.

163. **Lewis K.** 2001. Riddle of biofilm resistance. Antimicrobial agents and chemotherapy **45:**999-1007.

164. **Davies DG, Parsek MR, Pearson JP, Iglewski BH, Costerton JW, Greenberg EP.** 1998. The involvement of cell-to-cell signals in the development of a bacterial biofilm. Science **280:**295-298.

165. **Brown MR, Collier PJ, Gilbert P.** 1990. Influence of growth rate on susceptibility to antimicrobial agents: modification of the cell envelope and batch and continuous culture studies. Antimicrobial agents and chemotherapy **34:**1623-1628.

166. **Gilbert P, Collier PJ, Brown MR.** 1990. Influence of growth rate on susceptibility to antimicrobial agents: biofilms, cell cycle, dormancy, and stringent response. Antimicrobial agents and chemotherapy **34:**1865-1868.